Macrophages stimulate epicardial VEGFaa to trigger cardiomyocyte proliferation in larval zebrafish heart regeneration

Finnius A. Bruton[1]* , Aryan Kaveh[1], Katherine Ross-Stewart[1], Gianfranco Matrone[1], Magdalena Oremek[2], Emmanouil G. Solomonidis[1], Carl Tucker[1], John Mullins[1], Mairi Brittan[1], Jonathan Taylor[3], Adriano Rossi[2], Martin Denvir[1].

[1]Centre for Cardiovascular Science, Queen's Medical Research Institute, University of Edinburgh, Edinburgh, United Kingdom.

[2]Centre for Inflammation Research, Queen's Medical Research Institute, University of Edinburgh, Edinburgh, United Kingdom.

[3]Department of Physics, University of Glasgow, Glasgow, United Kingdom.

Corresponding author: *

Abstract

Cardiac injury induces a sustained innate immune response in both zebrafish and mammals. Macrophages, highly plastic immune cells, perform a range of both beneficial and detrimental functions during mammalian cardiac repair yet their precise roles in zebrafish cardiac regeneration are not fully understood. Here we characterise cardiac regeneration in the rapidly regenerating larval zebrafish laser injury model and use macrophage ablation and macrophage-less *irf8* mutants to define the requirement of macrophages for key stages of regeneration. We found macrophages to display cellular heterogeneity and plasticity in larval heart injury as in mammals. Live heartbeat-synchronised imaging and RNAseq revealed an early proinflammatory macrophage phase which then resolves to an anti-inflammatory, profibrotic phase. Macrophages are required for cardiomyocyte proliferation but not for functional or structural recovery following injury. Macrophages are specifically recruited to the epicardial-myocardial niche, triggering the expansion of the epicardium which upregulates mitogen VEGFaa. Experimental perturbation of VEGF signalling confirmed VEGFaa to be an important inducer of cardiomyocyte proliferation revealing

a previously unrecognised mechanism by which macrophages aid cardiac regeneration.

Introduction

Zebrafish are highly regenerative, exhibiting the capacity to restore full structure and functionality of a wide range of different tissues following injury or degeneration[1–5]. Cardiac injury is one such example where adult mammals are only able to facilitate maladaptive repair whilst zebrafish exhibit full tissue regeneration[6,7]. In humans, the most clinically severe form of cardiac injury is myocardial infarction (MI), where occlusion of a coronary artery triggers ischemic injury to the myocardium leading to the loss of approximately 1 billion cardiomyocytes[8]. Adult mammalian cardiomyocytes are considered post-mitotic, switching to hypertrophic growth shortly after birth and are therefore unable to restore lost myocardium which is instead replaced with non-contractile scar tissue[9]. MI patients suffer a sequel of maladaptive remodelling leading to left ventricular dilation and thinning of the scar further decreasing the function of the heart[10,11]. Therefore, there is a need for medical innovation which can reverse this process.

In contrast to mammals, apical resection and cryoinjury models of MI in zebrafish show full regeneration of lost myocardium via the dedifferentiation and proliferation of surviving cardiomyocytes[12,13]. Cardiac regeneration is complex and dynamic, with zebrafish hearts undergoing debridement of dead myocardium, followed by transient fibrosis, revascularisation and subsequent replacement of cardiomyocytes[14]. The inflammatory response has been demonstrated to be crucial for each of these key events, both in zebrafish and also other regenerative species such as axolotls and neonatal mice[15–17]. Innate immune cells ‘macrophages’ have emerged as important regulators of tissue regeneration. Indeed macrophage ablation has been shown to abrogate regeneration across multiple organs and organisms, including the zebrafish heart[15,16,18–22].

However, the precise contribution of macrophages to cardiac repair has been complicated by disparate results following macrophage perturbation in murine models of MI[7,23–25]. This is in part attributed to substantial heterogeneity of macrophage

subtypes and individual phenotypic plasticity[26,27]. Incidentally it is these same qualities that make macrophages ideally suited to modulating the dynamic signalling and cellular patterning of cardiac regeneration. Hence, macrophages are understood to exist on a multidimensional spectrum of phenotypes, informed both by the interaction environmental stimuli and ontological memory[28]. Recent studies have confirmed the presence of macrophage subsets in zebrafish yet their functional niche and interactions with other key cell types of the heart, such as the epicardium, remain poorly understood[29,30].

Larval zebrafish regenerate more rapidly than adults, occurring in just 48 hours after cardiac laser injury in 3-day old larvae[31,32]. Combined with their amenability for live *in vivo* imaging and genetic tractability, this model becomes a powerful tool with which to carefully examine how macrophages support multiple aspects of cardiac regeneration.

Here we perform an in-depth characterisation of several key processes in larval zebrafish cardiac regeneration, finding the heart regeneration program between the larvae and adult to be highly conserved. Perturbation of macrophage presence following injury using metronidazole-nitroreductase ablation or the macrophage null *irf8-/-* mutant[33] demonstrated a requirement for these cells in removal of apoptotic cells, epicardial activation and cardiomyocyte proliferation. We found that epicardial VEGFaa is required to induce cardiomyocyte proliferation following injury. Macrophages invade the epicardial-myocardial niche and ablation of macrophages prior to injury blocks epicardial expansion, preventing an increase of VEGFaa expression and therefore precluding cardiomyocyte proliferation.

Results

Macrophages display cellular heterogeneity following cardiac injury

We have previously demonstrated a sustained macrophage response to cardiac injury in zebrafish larvae[32] but it is not yet known if these cells are heterogenous and contain subsets. Thus the heterogeneity of macrophages following tissue injury is limited to a

99 handful of studies where fluorescent reporter lines have been combined to visualise
100 subsets[18,29,30,34]. To assess macrophage heterogeneity following cardiac injury, we
101 crossed the widely used zebrafish pan macrophage reporter line *Tg(mpeg1:GFP)* with
102 *Tg(csf1ra:gal4;UAS:mCherry-NfsB)* (shortened here to csf1ra: mCherry). csf1ra
103 (colony stimulated factor 1 receptor) is a cytokine required for macrophage
104 development and used as a macrophage reporter promotor in mammals.
105
106 Larval hearts were lasered at the ventricular apex at 72 hours post-fertilisation (hpf)
107 and subsequently imaged at 2, 6, 24, and 48 hours post injury (hpi) timepoints (Figure
108 1a). Macrophages migrate to the injured ventricular apex within two hours, peak at 6
109 and maintain elevated numbers until 48 hpi (Figures 1b & 1c). We found not all
110 recruited macrophages were co-positive for both transgenes, leading to three subsets
111 1) mpeg1+csf1ra- (19.3±5.1%), 2) mpeg1-csf1ra+ (2.8±2.1%) and 3) mpeg1+csf1ra+
112 (77.9±5.7%). Similar dynamics were seen for subsets 1 & 3 but since mpeg1-csf1ra+
113 were exceedingly rare (most often not present at all in injured hearts) it is not possible
114 to know if the dynamics are likewise similar. Both subsets exhibit a range of
115 morphologies with no overt difference (Figure 1d, Video 1). Whole-larva
116 epifluorescence images revealed an anterior-posterior gradient of co-positivity, with
117 most macrophages being mpeg1+csf1ra+ anteriorly and decreasing *csf1ra*:mCherry
118 positivity toward the tail (Supplementary Figure 1a). Taken together, our data
119 demonstrate that larval macrophages recruited to cardiac injury are heterogenous in
120 their markers, similar to adult zebrafish and mouse models[23,34].
121
122 **Macrophages display cellular plasticity following cardiac injury**
123
124 Macrophages also display remarkable plasticity in their phenotypes, changing
125 activation states via enhancer landscapes in response to extrinsic stimuli[27]. In
126 zebrafish, *tnfα* has emerged as a convenient marker for inflammatory macrophages,
127 with several studies reporting their importance for a tissue regeneration in a variety of
128 tissues[18,21,30].
129
130 We therefore performed cardiac laser injury on *Tg(tnfα:GFP;mpeg1:mCherry)* larvae,
131 finding a subset of mpeg1+ macrophages to be marked by *tnfα*:GFP expression

132 (Figure 1e). Quantification of tnfα+ macrophage number revealed this subset is
133 transient, found only at the 24 hpi timepoint and rarely in uninjured larvae (Figure 1g).
134 At the 24 hpi, tnfα+mpeg1+ macrophages make up just 19.3±4.9% of macrophages
135 whereas the majority (71.8±6.2%) are tnfα-mpeg1+ (Supplementary figure 1b).
136 Surprisingly, the remaining 8.8±4.1% of injury-recruited cells are tnfα+mpeg1-,
137 displaying macrophage morphology and behaviour.
138
139 We reasoned that if these tnfα+ macrophages were indeed inflammatory
140 macrophages then it should be possible to increase their abundance via application of
141 M1-polarisation cytokine IFN-γ. A single intravenous injection of zebrafish
142 recombinant protein IFN-γ-rel immediately prior to cardiac injury increased the
143 proportion of tnfα+mpeg1+ macrophages from 26.4±11.0% in PBS injected controls to
144 78.8±9.5%, supporting the idea that these are inflammatory macrophages
145 (Supplementary figure 1c-e).
146
147 To verify whether this is plasticity at the level of individual cells or recruitment of a pre-
148 polarised subtype, we performed *in vivo* imaging live in the beating heart. Timelapse
149 imaging clearly showed recruited macrophages becoming tnfα:GFP+ after arrival at
150 the injured ventricle, confirming that this represents an *in situ* conversion (Figure 1g,
151 Supplementary video 2). Conversely, we also observed an instance of a tnfα+mpeg1+
152 arriving at the injured ventricle pre-converted (Figure 1g). Finally, we observed that
153 macrophages appear to retract pseudopods and become spherical once arriving at
154 the ventricle (Supplementary figure 1f).
155
156 **Metronidazole-nitroreductase ablation and *irf8*-/- mutants provide a macrophage**
157 **null injury setting**
158
159
160 We next sought to understand what role macrophages are playing in the regeneration
161 of the larval heart, which occurs after just 48 hours[31,32]. To test this, we used two
162 completely different methods to induce macrophage-less hearts. Firstly we used the
163 *Tg(csf1ra:gal4;UAS:mCherry-nfsB)* line that expresses a nitroreductase enzyme 'nfsB'
164 in macrophages, leading to cell-specific apoptosis when exposed to prodrug

165 metronidazole[35]. We were able find dose that ablated macrophages but left other cells
166 such as neutrophils unaffected (Figure 2b & 2c, Supplementary figure 2a-d) and able
167 to respond to wounds (Supplementary figure 2e). We were able completely abolish
168 macrophage recruitment, with only mpeg1+/csf1ra+ cells being 1-2 apoptotic bodies
169 of resident cardiac macrophages (Figure 2a & 2d).
170
171 The second method was the use of the macrophage null *irf8*-/- mutant. This mutant
172 lacks the expression of irf8, a transcription factor required for macrophage
173 development. This mutation generates macrophage null animals which are otherwise
174 phenotypically normal (Figure 2e, Supplementary figure 3a-e)[33]. Presence of the
175 mutation was verified both the presence of the mutation by PCR (Figure 2f) and the
176 absence of macrophages by vital stain neutral red (Figure 2g). Both models therefore
177 provide powerful tools to dissect the role of macrophages in heart regeneration in
178 larval zebrafish.
179
180
181 **Macrophages contribute to the removal of apoptotic cardiomyocytes following**
182 **injury**
183
184 The best-known function of macrophages is the removal of dead cells as part of tissue
185 homeostasis but also following tissue injury[36]. We therefore endeavoured to
186 characterise cell death dynamics in our model of cardiac regeneration as well as the
187 requirement of macrophages in the removal of cellular debris.
188
189 Using the line *Tg(myl7:mKateCAAX;myl7:h2b-GFP)* that labels cardiomyocyte
190 sarcolemma and chromatin respectively, we observed that following injury, a circlet of
191 cardiomyocytes with pyknotic nuclei forms around the lesion site (Figure 3a). These
192 pyknotic nuclei were TUNEL+ at 6 hpi, confirming apoptosis and mirroring the
193 apoptotic border zone observed in mammalian infarcts[14,37] (Figure 3b). Interestingly,
194 endogenous fluorescence is lost from the lesion as early as 0.5 hpi (Figure 3c). We
195 hypothesised that the epicentre of the laser lesion may contain cells that immediately
196 die upon injury by necrosis. To test this, the membrane-impermeable, fluorescent DNA
197 intercalator propidium iodide (PI) was injected intravenously immediately following
198 injury (<0.5 hpi) to label necrotic cells. We found that there were indeed PI+ cells in

199 the GFP- region and PI+ debris scattered across the proximal myocardium from 1 hpi
200 (Figure 3d).
201
202 To discover how quickly this necrotic debris was cleared we used heartbeat-
203 synchronised light sheet microscopy[38] to image the injured heart of PI-injected
204 *Tg(mpeg1:GFP;myl7:h2b-GFP;myl7:mKateCAAX)* larva in timelapse. Necrotic cells
205 are cleared rapidly within the first 0-2 hpi (Figure 3e, Video 3). We also observed
206 condensed necrotic cells squeezing out from the myocardium into the pericardial
207 cavity, independently of macrophage contact (Video 3). In a similar time-lapse
208 experiment we imaged injured *Tg(myl7:mKateCAAX;myl7:h2b-GFP)* larva to see how
209 quickly cells start to condense their nuclei as part of programmed cell death. We found
210 that this too occurs extremely rapidly and is noticeable within just 1.5 hpi (Figure 3f,
211 Video 4).
212
213 To test if macrophages aid in removal of damaged myocardium we performed time-
214 lapse imaging at a later timepoint (4hpi) in injured *Tg(myl7:GFP;mpeg1:mCherry)*
215 larvae. By 3D surface rendering the GFP+ cardiomyocytes and mCherry+
216 macrophages we observed small GFP+ pieces of debris near the GFP- lesion being
217 removed and internalised by macrophages (Figure 3g, Video 5).
218
219 To determine if macrophages are required for the removal of apoptotic cells, we
220 performed TUNEL staining on *irf8*-/- and *irf8*+/+ *Tg(myl7:h2b-GFP)* larvae at the
221 standard 2, 6, 24, 48 hpi timepoints (Figure 3h &3i). In injured *irf8*+/+ hearts, the
222 number of apoptotic cardiomyocytes significantly increased at 2 hpi and 6 hpi
223 compared to uninjured controls (4.1±0.9 vs 0.0±0.0 and 5.3±1.0 vs 0.1±0.1
224 respectively). By 24 hpi, apoptotic cardiomyocytes are no longer significantly
225 increased in injured *irf8*+/+ hearts (0.01±0.01 uninjured vs 0.2±0.1 injured). However,
226 although injured macrophage-null *irf8*-/- hearts begin with a similar pattern of cell death
227 at 2hpi and 6hpi (5.5±0.8 & 5.9±0.9 apoptotic cardiomyocytes respectively), apoptotic
228 cardiomyocyte cells are still present at 24 hpi, returning to uninjured levels by 48 hpi.
229
230 In the macrophage ablation model, we saw a similar pattern of results where the
231 numbers of apoptotic cells are negligible in uninjured hearts of all treatment groups

232 but peak at 6 hpi in injured groups (NTR+met-, NTR-met+ & NTR+met+ =6.4±0.5,
233 6.4±0.5 & 6.0±0.5) (Figure 3J). By 24 hpi the non-ablated control groups had no longer
234 possessed significantly increased numbers of TUNEL+ myocardial cells (NTR+met- =
235 0.4±0.3 & NTR-met+ = 0.08±0.08) (Figure 3h & 3j). However, the injured macrophage-
236 ablated group showed a retention of apoptotic cells at 24 hpi (NTR+met+ = 1.5±0.3)
237 that resolved by 48 hpi. These results confirm the finding in the *irf8-/-* model that
238 macrophages are required for the timely removal of apoptotic myocardial cells.
239
240
241 **Macrophages are not required for structural or functional recovery of the heart**
242
243 In adult zebrafish models of myocardial infarction there is full restoration of contractility
244 and structure within 30-60 days[37]. It was therefore important to determine if there was
245 full structural and functional recovery in the larval model of cardiac injury and if this
246 was macrophage-dependent.
247
248 We lasered *Tg(myl7:GFP)* larvae in the macrophage ablation model. Using heartbeat-
249 synchronised LSFM it was possible to acquire detailed 3D scans of cardiac structure
250 of individual larvae across multiple timepoints (Figure 4a). In all treatment groups, the
251 lesion remained the same size (~750μm^2) between 2 hpi and 6 hpi, with no difference
252 between groups. By 24 hpi this lesion had almost completely regressed (95% to
253 37.1μm^2±24.4) in macrophage replete NTR+met- larvae (Figure 4b). However, in both
254 the macrophage ablated NTR+met+ and the other macrophage replete NTR-met+
255 larvae, lesion closure was slightly delayed at 24 hpi (73% and 75% to 234.7±59.7 μm^2
256 and 221.4±84.6 μm^2 respectively). By 48 hpi the lesions of larvae from each group
257 had entirely regressed and luminal surface renders of injured ventricles showed
258 normal trabecular structure (Figure 4a). These results suggest macrophages are not
259 required for lesion closure, but that metronidazole-treatment slightly delays this
260 process.
261
262 We next sought to understand if this was also true of cardiac function. Again using
263 *Tg(myl7:GFP)* larvae, we acquired lateral-view videos of beating hearts by
264 epifluorescence, and calculated ventricular ejection fraction (Figure 4c &

265 Supplementary Figure 4a & 4b). Immediately following injury at 2 hpi ejection fraction
266 is severely depressed in all groups from ~74% in uninjured ventricles to ~54% in
267 injured. Ejection fraction recovers quickly by 6 hpi, with none of the treatment groups
268 being significantly different to their respective uninjured controls but there still being a
269 strong trend for injured larvae to have decreased ejection fraction (~78% injured vs
270 87% uninjured). At 24 hpi and 48 hpi this trend is also gone for all treatment groups
271 and injured hearts are functionally indistinguishable from uninjured hearts. This data
272 suggests that injured larval hearts recover their function rapidly and that this recovery
273 is not macrophage dependent.
274
275 We next performed identical experiments examining the recovery of cardiac structure
276 and function with *Tg(myl7:GFP)* larvae on an *irf8* mutant background. Both *irf8*+/+ and
277 *irf8*-/- genotype larvae showed substantial lesion regression (~80%) between 6 hpi
278 and 24 hpi (898.6 $\mu m^2 \pm 189.7$ to 211.6 $\mu m^2 \pm 115.8$ vs 1002.9 $\mu m^2 \pm 158.4$ to 113.89
279 $\mu m^2 \pm 59.5$ respectively) (Figure 4d & 4e). No difference in lesion size was seen at any
280 timepoint and both genotypes had completely closed their lesions by 48 hpi. Normal
281 trabecular structure was seen in both groups at 48 hpi following full structural recovery
282 (Figure 4d). The recovery of ejection fraction in this model followed the same trend as
283 that of the metronidazole-nitroreductase model, with the ejection fraction of injured
284 larvae indistinguishable from uninjured larvae by 24 hpi in both genotypes (Figure 4e).
285 Our near identical findings in the *irf8* macrophage null model confirm that larval hearts
286 rapidly recover following laser injury and this is macrophage independent.
287
288 Finally, we wished to understand the mechanism of lesion closure, particularly how it
289 was able to occur so rapidly following laser injury. We performed heart synchronised
290 time-lapse imaging of lesions immediately following injury in *Tg(myl7:GFP)* larvae.
291 Surface rendering of 3D scans of heart facilitated interpretation of morphological
292 changes in myocardial volume (Figure 4g, Video 6). We observed GFP+ myocardial
293 budding on opposite sides of the lesion border zone and subsequent invasion into the
294 lesion, adhering to form a bridge. In order to ascertain if these buds and bridges
295 represented individual pioneer cardiomyocytes, we repeated these live imaging
296 experiments in *Tg(myl7:h2b-GFP;myl7:mKateCAAX)* larvae, facilitating the tracking of
297 individual cardiomyocytes by virtue of their labelled nuclei and plasma membranes

298 (Figure 4h, Video 7). The initially disorganised surviving cardiomyocytes bordering the
299 lesion began to extend protrusions into the lesion until they adhere with other single
300 cardiomyocytes bridging from the opposing side of the lesion.
301
302 **Macrophage ablation abolishes injury-associated increase in cardiomyocyte**
303 **proliferation**
304
305 To test if laser injury increases cardiomyocyte proliferation, we performed EdU staining
306 in *Tg(myl7:h2b-GFP)* larvae in two experiments. The first where uninjured and injured
307 larvae were exposed to EdU during 0-24 hpi and the second where the exposure
308 occurs 24-48 hpi (Figure 5a). Analysis of the proportion of h2b-GFP+ with EdU
309 incorporation immediately following the EdU pulse indicated the presence of cycling
310 cardiomyocytes over both days (Figure 5b & 5c). EdU incorporation into
311 cardiomyocyte nuclei was organ-wide, most often seen in pairs of cardiomyocytes but
312 with no obvious distal or proximal localisation relative to the lesion (Figure 5b).
313 Comparison between uninjured and injured hearts revealed no significant difference
314 in the proportion of EdU+ cardiomyocyte nuclei 0-24 hpi (21.3±3.3 vs 18.9±3.4
315 respectively) (Figure 5c). However, over 24-48 hpi there was 35% increase in the
316 proportion of EdU+ cardiomyocytes in injured hearts relative to uninjured (43.5±1.8%
317 vs 32.2±2.0% respectively). Timelapse *in vivo* imaging of dividing cardiomyocytes
318 showed nuclear division followed by cytokinesis, exclusively giving rise to
319 mononuclear cells with no obvious hypertrophy (Video 8, Supplementary Figure 5a).
320
321 In order to understand if macrophages are required for the injury-dependent increase
322 in cardiomyocyte proliferation we EdU pulsed only over the proliferative 24-48 hpi
323 window in the macrophage-less models (Figure 5d). In the metronidazole-
324 nitroreductase ablation model we found that the percentage of EdU+ cardiomyocytes
325 increased in injured hearts in both the NTR+met- and NTR-met+ control groups but
326 not in the macrophage-ablated NTR+met+ (Figure 5e & 5f). This result indicates that
327 macrophages are a requirement for injury-dependent increase in cardiomyocyte
328 proliferation. However, in contrast to the metronidazole-nitroreductase model, analysis
329 of cardiomyocyte proliferation in *irf8-/-* mutants revealed that they too significantly
330 increased the percentage of EdU+ cardiomyocytes following injury, comparably to

331 *irf8+/+* larvae (Figure 5g & 5h). To resolve this disparity, we examined more closely
332 the differences between these models. We found, like others, that *irf8-/-* mutants
333 possess a greater global number of neutrophils than *irf8+/+* and mount a larger
334 neutrophil response to injury (Supplementary Figure 5b & 5c). Since we do not
335 observe an increased neutrophil response in NTR+met+ larvae, we hypothesised that
336 neutrophils might be compensating for macrophages in *irf8-/-* larvae (Supplementary
337 Figure 5d). To test this hypothesis, we inhibited neutrophil recruitment in *irf8-/-* larvae
338 using a well-established antagonist 'SB225002' which blocks CXCR1/2 activation, a
339 key chemokine receptor for neutrophil migration. CXCR1/2 inhibition successfully
340 lowered the number of recruited neutrophils (2.0±3.4 vs 0.43±0.18) and abolished
341 injury associated increase in cardiomyocytes in *irf8-/-* (Supplementary Figure 5e-g).
342 Taken together this suggests that macrophages are important in inducing
343 cardiomyocyte proliferation but are not an absolute requirement and can be
344 substituted for by excess neutrophils.
345
346 **Cardiac injury induces epicardial activation and VEGFaa upregulation**
347
348 Macrophages are known to secrete a variety of growth factors and cytokines following
349 cardiac injury but it is controversial whether these factors are directly required for
350 cardiomyocyte proliferation *in vivo*[39,40]. We thought it plausible that macrophages may
351 be releasing a key mitogen following laser injury. VEGFaa has recently been
352 demonstrated to drive cell cycle entry in adult zebrafish following cryoinjury and is
353 highly expressed in macrophages in larval trunk injury[21,41]. We hypothesised that
354 macrophages may be promoting cardiomyocyte proliferation via the release of
355 VEGFaa mitogen. Therefore we performed laser injury in
356 *Tg(vegfaa:GFP;mpeg1:mCherry)* larvae to examine potential colocalised expression.
357 However, no vegfaa expression was observed in macrophages at any timepoint, in
358 uninjured or injured hearts (Supplementary Figure 6a & 6b).
359
360 In contrast, substantial vegfaa expression was observed in mesothelial cells overlying
361 the myocardium (Figure 6a). Colocalisation with established epicardial marker tcf21 in
362 *Tg(tcf21:DsRed;vegfaa:GFP)* larvae confirmed these cells to be early epicardium
363 (Figure 5b). We tested if epicardial vegfaa:GFP expression increased still further

364 following larval cardiac injury by fluorescence intensity analysis of 3D *in vivo* imaging.
365 vegfaa:GFP intensity increased significantly at 48 hpi with a strong trend to increase
366 at 24 hpi (Figure 6d & 6e). Quantification of the total number of ventricular epicardial
367 cells revealed that both the number of cells and their individual vegfaa:GFP expression
368 increased following cardiac injury (Supplementary Figure 6c & 6d)
369
370 **Macrophages localise to the epicardial niche and induce epicardial expansion**
371
372 Since macrophages did not appear to express this known mitogen themselves, we
373 wondered if their presence might be required to induce VEGFaa expression in
374 epicardium. Supporting this hypothesis, detailed 3D analysis of macrophage
375 localisation following injury showed recruited macrophages to synapse with epicardial
376 cells by invading the myocardial-epicardial niche (Figure 6e). Given macrophage
377 ablation abolishes injury-dependent cardiomyocyte proliferation (Figure 5f), we used
378 metronidazole-nitroreductase model to ablate macrophages and assess whether
379 epicardial activation still occurs following injury. We found that following injury,
380 increased vegfaa:GFP expression was observed both NTR-met+ and NTR+met-
381 groups but this failed to occur in NTR+met+ hearts, with vegfaa:GFP expression not
382 significantly higher than in uninjured (Figure 6f & 6g). Interestingly, macrophage
383 ablation did not affect vegfaa:GFP expression per cell but did block the expansion of
384 epicardial cell number following injury (Figure 6h & Supplementary Figure 6e). Our
385 data therefore suggests that recruitment of macrophages to epicardium is required for
386 subsequent epicardial activation and expansion, as well to increase in net cardiac
387 vegfaa expression.
388
389 **VEGFaa is both required for, and sufficient for, cardiomyocyte proliferation in**
390 **larval zebrafish**
391
392 Although VEGFaa has been shown to be a potent inducer of cardiomyocyte
393 hyperplasia in adult zebrafish and hypertrophy in adult mice, it is not known whether
394 this is also true in larval zebrafish[41–43]. We first tested if VEGFaa alone is sufficient to
395 stimulate cardiomyocyte proliferation in the absence of cardiac injury. Recombinant
396 zebrafish VEGFaa protein (zfVEGFaa) or PBS control solution was microinjected into
397 circulation via the sinus venosus of 72 hpf *Tg(myl7:h2b-GFP)* larvae and total

398 cardiomyocyte number assessed at 24 and 48 hpt (Figure 7a). A single injection of
399 zfVEGFaa at 3 dpf increased total cardiomyocyte number by 13.3% relative to PBS-
400 injected controls at 24 hpi (Figure 7b & 7c). Interestingly, by 48 hpt this is no longer
401 statistically significantly different. This data confirms that VEGFaa is sufficient to
402 stimulate hyperplasia in larval zebrafish hearts.
403
404 To test if VEGF signalling is required for the injury-associated cardiomyocyte
405 proliferation, we used a pan-VEGFR receptor antagonist AV951 (Tivozanib) to block
406 VEGF signalling. AV951 is a highly potent small molecule inhibitor and is widely used
407 in larval zebrafish angiogenic assays as it can be easily delivered to tissues via
408 bathing, commonly at concentrations of 500nM[44,45]. Our own validation and dose
409 optimisation of VEGFR inhibition via a larval-laser trunk injury neovascularisation
410 model[21] found AV951 could completely abolish neovascularisation in skeletal muscle
411 at doses as low as 10nM (Supplementary Figure 7a-c). Consequently, we bathed
412 larvae in 10nM AV951 dose over the course of our cardiac injury model, pulsing with
413 EdU at 24-48 hpi and quantifying EdU+ cardiomyocytes at 48 hpi (Figure 7d).
414 Interestingly, AV951 decreased the proportion of EdU+ cardiomyocytes in both the
415 uninjured and injured groups (uninjured 38.4±3.4 vs 28.0±3.0 and injured 42.9±3.8 vs
416 31.6±2.2) (Figure 7e & 7f). This suggests that VEGF signalling in the heart is required
417 for cardiomyocyte proliferation both as part of normal development and following
418 cardiac injury. This agrees with our previous identification of constitutive epicardial
419 VEGFaa expression in uninjured hearts.
420
421 **Notch and Nrg-ErbB signalling are required for cardiomyocyte proliferation**
422
423 Following the finding that VEGFR signalling is required for cardiomyocyte proliferation
424 in both uninjured and injured hearts, we next sought to examine potential downstream
425 effectors. Strong candidates were notch and neuregulin-ErbB signalling pathways.
426 Notch signalling has been shown to be required for adult heart regeneration and
427 cardiomyocyte proliferation in adult zebrafish[46–48] as well as in zebrafish heart
428 development[49]. Neuregulin is a potent cardiac mitogen and has similarly been shown
429 to be essential for adult regeneration as well as larval heart development[50–54].

430 Therefore, we first examined if either of these signalling pathways were required for
431 cardiomyocyte proliferation in the larval heart following injury.
432
433 The gamma secretase inhibitor DAPT ((N-[N-(3,5-difluorophenacetyl)-l-alanyl]-S-
434 phenylglycine t-butyl ester) has been successfully used as a pan-notch inhibitor for
435 over two decades and has been demonstrated in both zebrafish and drosophila to
436 phenocopy various notch mutants[55–57]. We performed the laser injury on
437 *Tg(myl7:nlsDsRed)* larvae, bathing them in either 100µm DAPT or a vehicle control
438 solution following injury and quantified total cardiomyocyte number at 48 hpi (Figure
439 7g). In agreement with previous studies, notch inhibition decreased cardiomyocyte
440 number in uninjured hearts by ~8% (253.3±5.2 vs 233.4±4.5) (Figure 7h & 7i).
441 Additionally, notch inhibition was similarly able to decrease cardiomyocyte number in
442 injured hearts (266±5.6 vs 229±3.6). These results confirm that notch signalling is
443 important for the expansion of cardiomyocyte number in both development and
444 following cardiac injury.
445
446 We repeated this experiment, this time bathing larvae in an ErbB2 antagonist AG1478
447 (Figure 7e). Small molecule inhibitor AG1478 selectively inhibits ErbB2, required co-
448 receptor for ErbB4 dimerization and subsequent neuregulin signal transduction.
449 AG1478 is widely used in zebrafish cardiac biology to inhibit neuregulin-ErbB
450 signalling[52,58–61], having been shown to faithfully phenocopy *erbb2* mutants[62].
451 Interestingly, the results exactly replicated those of the notch inhibition experiment,
452 with decreased cardiomyocyte number in both uninjured (257.2±5.8 vs 235.2±4.2) and
453 injured hearts (265.7±5.5 vs 229±5.9) (Figure 7j &7k). These results suggest that, like
454 notch signalling, neuregulin-ErbB signalling is required for the expansion of
455 cardiomyocyte number in both uninjured and injured settings.
456
457 **Cardiac injury and VEGFaa induce endocardial notch signalling**
458
459 Having demonstrated individual requirements for VEGF, notch and neuregulin-ERBB
460 signalling, we were keen to test if they act in one pathway.
461

462 To reveal the epistatic relationship of these signalling components, we designed an
463 experiment utilising the notch signalling reporter line *Tg(Tp1:venus-PEST)* as a
464 readout of notch expression. The peptide sequence 'PEST' targets the fluorophore
465 venus for rapid degradation and so increases temporal resolution of gene expression
466 patterns. Recombinant zfVEGFaa or PBS control solution was injected into 3 dpf
467 larvae and hearts analysed by heart-synchronised light-sheet microscopy for changes
468 in notch signalling at 6, 24 and 48 hpi (Figure 8a). Furthermore, an additional group of
469 larvae were injected with zfVEGFaa but also bathed in ErbB2 antagonist AG1478. We
470 hypothesised a VEGFaa->notch->Nrg-ERBB pathway hierarchy (Figure 8b) and
471 therefore reasoned that zfVEGFaa injection should upregulate notch signalling but that
472 inhibition of Nrg-ErbB signalling should be unable to suppress zfVEGFaa-induced
473 notch upregulation.
474
475 In agreement with previous studies[63,64] we found that in PBS-injected larvae, notch
476 signalling was primarily in the endocardium, colocalising with endothelial reporter
477 kdrl:mCherry, and in the occasional cardiomyocyte (Figure 8b). Notch signalling in
478 larval cardiomyocytes has been recently shown to be the result of lateral inhibition
479 during trabeculation whereas endocardial notch is known to drive cardiomyocyte
480 proliferation[63]. Interestingly, endocardial notch signal was relatively low and only
481 detectable in a subset of larvae at any given timepoint (Figure 8c). We therefore
482 assessed if the percentage of hearts with Tp1:venus-PEST+ (notch+) endocardium
483 increased following zfVEGFaa injection. zfVEGFaa injection significantly increased
484 the percentage of notch+ endocardium from 46.4% to 78.6% at 6 hpi. Though there
485 was a trend for the percentage of notch+ hearts to be higher in zfVEGFaa-injected
486 larvae at 24 hpi (35.7% vs 17.9%), it did not reach statistical significance, nor was any
487 difference observed at 48 hpi.
488
489 Treatment of zfVEGFaa-injected larvae with AG1478 failed to block the increase in the
490 percentage of notch+ hearts. Furthermore, zfVEGFaa+AG1478 treated larvae had a
491 substantially higher percentage of notch+ hearts at 48 hpi than those treated with
492 zfVEGFaa alone (25.0% vs 0%). Together, these results show that VEGFaa is
493 upstream of endocardial notch signalling and is that notch is unaffected by neuregulin-
494 ErbB inhibition, excluding it from being downstream of the latter. Furthermore, the
495 increased notch-signalling observed in zfVEGFaa+AG1478 hearts is highly suggestive

496 of negative-feedback, supporting the hypothesis that neuregulin might be downstream
497 of notch as seen cardiac development.
498
499 Next, we sought to confirm if these signals interacted in a similar manner following
500 injury; in particular whether injury alone could induce the same patterns of signalling.
501 The experiment was repeated, substituting zfVEGFaa injection with laser injury (Figure
502 8e). As with zfVEGFaa injection, laser injury also increased the percentage of hearts
503 with notch+ endocardium but this occurred later, at 48 hpi (50.0% vs 11.1%) (Figure
504 8f & 8g). Furthermore, there was also a strong trend for increased percentage of
505 notch+ hearts in injured hearts relative to uninjured hearts at 24 hpi. Similar to
506 zfVEGFaa injection, AG1478 did not block notch signalling, rather it seemed to
507 enhance it. Whilst the percentage of notch+ hearts in the injured group did not
508 significantly increase by 24 hpi, injured+AG1478 treated larvae did significantly
509 increase relative to uninjured larvae (52.9% vs 11.1%). Furthermore, there was a trend
510 for a greater percentage of notch+ hearts in injured+AG1478 treated larvae at 48 hpi
511 compared to injured larvae alone (61.1% vs 50.0%). Taken together, these results
512 demonstrate that endocardial notch signalling is downstream of cardiac injury and
513 VEGFaa but is not downstream of Nrg-ErbB signalling, suggesting the latter is likely
514 operating downstream of notch.
515
516 **Regenerating larval hearts resolve inflammation and enter a reparative stage by**
517 **48 hpi**
518
519 To understand what transcriptional changes are still occurring by the final timepoint of
520 our model, we performed bulk RNAseq on pooled uninjured and injured larval hearts
521 at 48 hpi (Figure 9a). We found a total of 1,464 differentially expressed (log_2 fold
522 change >1) genes, 418 were upregulated in injured and 1,046 downregulated in
523 injured hearts. We did not observe differential expression of canonical markers of
524 proliferation such as MCM2, mKi67 and PCNA suggesting that the proliferation we
525 observe from 24 hpi is concluded by 48 hpi (Figure 9b). In agreement with this, gene
526 ontology analysis indicated categories such as growth factors and cell proliferation not
527 to be enriched at 48 hpi (Supplementary Figure 9e). Although not differentially
528 expressed at 48 hpi, many of the ligands and cognate receptors for VEGF, Nrg-ErbB

529 and notch were highly expressed in both uninjured and injured hearts indicating that
530 these pathways are active in the larval heart (Supplementary table 1).
531
532 Most inflammatory and M1 markers were either not differentially expressed or
533 downregulated in injured hearts, such as Il1b (Figure 9b & Supplementary file 1). In
534 contrast, we found injury-associated upregulation of 39 collagen isoforms, and several
535 profibrotic genes such as tgfb1a, osteopontin and markers of epithelial to
536 mesenchymal transition (EMT) such as vimentin and twist2-3. Similarly, hierarchical
537 clustering of differentially expressed genes revealed 9 distinct clusters with Cluster 1
538 being upregulated in injured hearts and enriched in collagens, matrix metalloproteins
539 (MMPs) and fibroblast growth factors (FGFs) (Figure 9c, Supplementary file 2).
540 Additionally, Cluster 2 contained several EMT genes, Cluster 8 genes relating to cell
541 recruitment and lymphagiogeneis whilst Cluster 7 contained several embryonic-
542 associated myosins and myosin binding proteins such as myl10, myl13 and cald1b.
543 Clusters 3-6 & 9 were downregulated in injury, Cluster 2 was enriched for immune
544 genes and Clusters 4 and 6 for growth factors, with Clusters 3 and 5 less easily
545 described.
546
547 Taken together, our RNAseq results suggest that the inflammatory and proliferative
548 stages are largely concluded by 48 hpi and that a pro-resolving, reparative and
549 remodelling phase dominates from this timepoint.
550
551 **Discussion**
552
553 In this study we present a detailed characterisation of the larval zebrafish model of
554 heart regeneration, demonstrating the heterogeneity and plasticity of macrophages in
555 cardiac injury and testing the requirement of macrophages for the removal of apoptotic
556 cells, cardiomyocyte proliferation, epicardial activation and recovery of cardiac
557 structure and function. Furthermore, we demonstrate the utility of the larval cardiac
558 injury model by taking advantage of it's *in vivo* cardiac imaging opportunities and
559 amenability to pharmacological intervention to suggest a novel role for macrophages
560 in driving cardiomyocyte proliferation via epicardial activation.
561

562 Recent zebrafish studies examining macrophages in other wound contexts, such as
563 spinal cord and tail transection, have demonstrated tnf-α to mark M1-like
564 macrophages, that then transition to M2-like macrophages[18,30,65]. Similarly, studies in
565 the adult zebrafish heart have shown the presence of a subsets stratified on the basis
566 of tnf-α, wt1b, csf1ra and mpeg1 transgenic reporter expression[29,34]. We confirmed
567 the presence of mpeg1+csf1ra+ and mpeg1+csf1ra- subsets in larval heart injury,
568 finding as in adults that these cells have identical recruitment dynamics and no obvious
569 differences in morphology or behaviour[34]. Recent Cre-Lox lineage tracing has shown
570 that mpeg1+csf1ra- cells have a non-haematopoietic origin, are csfr1a-independent
571 developmentally and unlike mpeg1+csf1ra+ cells, are not phagocytic[66,67]. Due to their
572 non-haematopoietic origin some have termed mpeg1+csf1ra- cells as 'metaphocytes'
573 rather than macrophages however macrophage ontogeny is diverse and environment
574 is known to play a leading role in establishing macrophage identity[27,68]. Therefore,
575 further functional analysis and transcriptomic clustering relative to other immune cells
576 is required to classify mpeg1+csf1ra- macrophages as a non-macrophage cell type.
577
578 Our observation of a transient tnfα+ subpopulation is in agreement with findings in the
579 adult cryoinjury and larval tail-transection models[30,34]. Our success in increasing the
580 percentage of tnf-α+ macrophages by canonical M1-polarising cytokine IFN-γ-rel
581 suggests that early tnf-α+ macrophages are proinflammatory. Furthermore, we used
582 heart synchronised live imaging to show that macrophages can convert from
583 mpeg1+tnf-α- to mpeg1+tnf-α+. This is the first time that macrophages have been
584 imaged converting phenotype in the heart and provides direct evidence of plasticity as
585 opposed to recruitment of heterogenous subsets. Our RNAseq data confirmed the
586 inflammatory response to be transient as by 48 hpi hearts downregulate inflammatory
587 cytokines and growth factors but upregulate collagens and reparative cytokines. Our
588 finding that the a fibrotic program is activated in injured hearts despite full structural
589 and functional recovery is in agreement with a recent study showing the scar-deficient
590 runx1-/- zebrafish to undergo successful cardiac regeneration[69]. It might be that the
591 fibrotic program is concomitantly activated upon the resolution of inflammation.
592
593 We used two separate methods to examine the effect of removing macrophages from
594 the larval heart injury model. By using two methods we hoped to control for potential

artefacts of the techniques. Cell death data acquired by either technique demonstrated that macrophages are required for the removal of apoptotic cells following injury. Furthermore, we found that the structure of laser lesions was analogous to that of human infarcts and adult zebrafish cryoinjury with a necrotic core surrounded by apoptotic cardiomyocytes and border zone[6,37]. Interestingly, these cells do eventually seem to be cleared even in the absence of macrophages. Our live imaging showed that dead cardiomyocytes can be expelled from the myocardium independently of macrophages. It is possible that this is a mechanical consequence of cardiac contraction however a similar phenomenon is known to occur in neuroepithelium where neurons appear to extrude apoptotic cells out of tissue[70,71]. Nevertheless, we were also able to image, for the first time, macrophages actively removing and internalising myocardial material following cardiac injury.

Surprisingly, we found that the absence of macrophages in neither macrophage-less model had any effect on the structural or functional recovery of the injured larval heart. This is in contrast to previous studies in mice where macrophage depletion leads to a reduced ejection and infarct expansion [23,72,73]. Likewise, liposomal clodronate macrophage ablation and CCR2-antagonist inhibition of macrophage recruitment in regenerative neonatal mice, zebrafish and axolotl hearts causes blocked or delayed resolution of the infarct area[15,16,74]. The contrasting results in the larval heart might simply be a consequence of its small size and low transmural pressure. Furthermore, the diameter of the infarct is only 1-2 cells, allowing surviving bordering cardiomyocytes to restore the myocardial syncytium without prior proliferation. Indeed, we observed individual cardiomyocytes extending protrusions into the lesion. Previous histological analysis of the border zone in injured adult zebrafish and neonatal mouse hearts has shown cardiomyocytes exhibiting a similar mesenchymal phenotype following partial dedifferentiation and disassembly of sarcomeres.[75–77]. To our knowledge, this is the first time this behaviour has verified directly by time-lapse imaging live in a beating heart.

Studies in adult zebrafish and neonatal mice have shown ablation of macrophages to decrease cardiomyocyte proliferation, the exception being axolotls where it has no effect[15,17,40,78,79]. Additionally, cardiomyocyte proliferation and macrophage recruitment dynamics correlate and enhancement of macrophage recruitment in the

629 non-regenerative teleost medaka, facilitates cardiomyocyte proliferation and
630 regeneration[17,78]. However, early revascularisation is critical for cardiomyocyte
631 proliferation and is macrophage-dependent calling into question whether
632 macrophages directly induce cardiomyocyte proliferaiton[17,80]. Our larval model
633 provided a unique opportunity to uncouple the angiogenic actions of macrophages
634 from cardiomyocyte proliferation since larval hearts do not have supporting
635 vasculature at this stage[32]. The increased proliferation we observed following injury
636 demonstrates that larval hearts are truly regenerating and not recovering via normal
637 developmental growth. Furthermore, macrophage ablation completely abolished the
638 injury-dependent cardiomyocyte proliferation seen in macrophage replete hearts,
639 suggesting this effect is might not be entirely mediated by revascularisation in other
640 models. Interestingly, *irf8-/-* larvae still exhibit a robust proliferative response to injury.
641 In line with previous studies, we found that *irf8-/-* and not macrophage-ablated larvae
642 showed increased recruitment of neutrophils[18,33]. Pharmacological inhibition of
643 neutrophil recruitment abolished expansion of cardiomyocyte number suggesting that
644 large neutrophil response can compensate for the absence of macrophages.
645
646 Zebrafish macrophages have been shown to upregulate VEGFaa following injury of
647 trunk intersegmental vessels and VEGFaa has also been shown to be a powerful
648 mitogen for cardiomyocytes in adult cryoinjury[21,41]. However, macrophages were not
649 VEGFaa+ in the vegfaa:GFP reporter line. We instead found that VEGFaa is
650 constitutively expressed in larval epicardium[41,81]. Pharmacological inhibition of
651 VEGFR signalling decreased cardiomyocyte proliferation in uninjured larvae and in
652 injured larvae who show an increase in expression of VEGFaa. This provides a
653 mechanism for epicardial driven cardiomyocyte proliferation. Confirming this, a single
654 intravenous injection of recombinant zfVEGFaa substantially increased the number of
655 cardiomyocytes in hearts at 24 hpt. Interestingly, control hearts appear to match this
656 increase by 48 hpt. It is possible that endogenous VEGFaa is therefore acting as a
657 trigger to cardiomyocytes competent to divide and that injection of zfVEGFaa triggered
658 the majority of these competent cardiomyocytes to divide ahead of developmental
659 schedule.
660
661 Although macrophages do not express VEGFaa themselves following cardiac injury,
662 their presence appears to be required for injury-dependent upregulation of mitogen

663 VEGFaa via the expansion of the epicardium. Furthermore, we showed that
664 macrophages specifically home to the myocardial-epicardial niche. This is reminiscent
665 of previous findings in developing and injured mouse hearts where yolk-derived and
666 Gata6+ pericardial cavity macrophages are recruited to the epicardium,
667 respectively[82,83]. Future studies should seek to identify precisely how macrophages
668 activate epicardium. Given we found that elevated neutrophil recruitment can induce
669 cardiomyocyte proliferation in the absence of macrophages, epicardial activation
670 might be induced by a shared inflammatory factor.
671
672 We showed both notch and Nrg-Erbb signalling to be required for expansion of
673 cardiomyocyte numbers in both uninjured and injured heart. This is in agreement with
674 previous findings in adult zebrafish and murine models[46–48,51,58]. Interestingly, our data
675 demonstrated that both VEGFaa and injury increase endocardial notch signalling.
676 Endocardial notch1b is known to regulate maturation of the larval ventricle via
677 downstream Nrg1[49]. Therefore, it was plausible that a VEGF>Notch>Nrg-ErbB
678 pathway might be inducing cardiomyocyte proliferation in the larval cardiac injury
679 model. A recent paper published during the course of this study demonstrated
680 exogenous VEGF to be capable of inducing cardiomyocyte hypertrophy in the mouse
681 heart via a VEGF>notch>nrg1 pathway[43]. Whilst unconfirmed in models of MI, it raises
682 the possibility that this could represent an injury-dependent recapitulation of
683 developmental growth programming, conserved between regenerative and non-
684 regenerative animals. Given the angiogenic effects of VEGFaa, our proposed pathway
685 would present an elegant coupling revascularisation to myocardial growth, under the
686 control of macrophage inflammation. Future studies are required to determine if this
687 pathway is similarly active in adult zebrafish and mammalian hearts and understand
688 precisely how macrophages are inducing upstream epicardial activation.
689
690
691 **Materials and Methods**
692
693 **Zebrafish husbandry and lines used**
694
695 Zebrafish husbandry and maintenance was conducted as per standard operating
696 procedures, in accordance with the Animals (Scientific Procedures) Act, 1986 and

697 approved by The University of Edinburgh Animal Welfare and Ethical Review Board in
698 a United Kingdom Home Office-approved establishment. All our experiments were
699 performed on staged zebrafish aged between 3 dpf and 5 dpf[84]. The following
700 transgenic and mutant lines were used: *Tg(myl7:eGFP)*^{twu26} [85], *Tg(mpx:mCherry)*^{uwm7}
701 [86], *Tg(mpeg1:mCherry)*^{gl23} [87], *Tg(mpeg1:eGFP)*^{gl22} [87], (*Tg(mpx:GFP)* ^{i114} [88],
702 *Tg(myl7:h2b-GFP)*^{zf52} [89], *Tg(myl7:mKateCAAX)*^{SD11} [90], *Tg(fms:Gal4.VP16)*^{i186},
703 referred to as csfr1a:gal4[91], *Tg(UAS-E1b:NfsB-mCherry)*^{c264} abbreviated to
704 UAS:NfsB-mCherry[92], *Tg(vegfaa:eGFP)*^{PD260} [41], *Tg(myl7:nlsDsRed)*^{f2} [93]
705 *Tg(TNFa:eGFP)*^{sa43296} [30], *Tg(Tp1:venus-PEST)*^{S940} [94], *Tg(kdrl:hsa.HRAS-*
706 *mCherry)*^{S896} [95], *Tg(kdrl:GFP)*^{la116} [96], *Tg(tcf21:DsRed)*^{PD37} [97],
707 *Tg(myl7:gal4:myl7:GFP)*^{cbg2Tg} [98], *Tg(UAS:mRFP)*[99] and irf8$^{st95/st95}$ [33] referred to as *irf8-*
708 */-.* Adults were day-crossed as appropriate to yield desired combinations of transgenes
709 in embryos. Embryos were treated with 0.003% phenylthiourea (Fisher Scientific) at 7
710 hpf to prevent pigment formation and therefore enhance image clarity[100]. Embryos and
711 larvae were incubated at 28.5°C in conditioned media/water (6.4 mM KCl, 0.22 mM
712 NaCl, 0.33 mM $CaCl_2 \cdot 2H_2O$, 0.33 mM $MgSO4 \cdot 7H_2O$) + 0.1% methylene blue (w/v)
713 and imaged at room temperature (23°C) using epifluorescence or light sheet
714 fluorescence microscopy (details below). When necessary, larvae were anesthetized
715 using 40 µg/ml tricaine methanesulfonate (Sigma Aldrich) in conditioned media.
716
717 **Cardiac laser injury**
718
719 A Zeiss Photo Activated Laser Microdissection (PALM) laser system (Zeiss) was used
720 to precisely cause a localised injury at the ventricular apex of anesthetized 72 hpf
721 larvae[32]. Larvae were mounted on a glass slide in 20 µl anesthetized conditioned
722 media and lasered via a 20X objective. Injuries were deemed successful and complete
723 once ventricular contractility decreased, the apex had shrunk, and the myocardial wall
724 had swollen without causing cardiac rupture and subsequent bleeding. A successful
725 cardiac injury results in the portion of dysfunctional tissue losing fluorescent
726 myocardial transgenic fluorescence signal. Uninjured larvae were treated in the same
727 manner up to the point of laser injury, when they were individually transferred into
728 single wells of a 24-well plate and maintained in the same environmental conditions
729 as injured fish.
730

731 **Epifluorescence microscopy**

732

733 Larvae were mounted laterally in conditioned media on a glass slide and imaged using
734 a Leica M205 FA stereomicroscope with GFP and mCherry filters. For all serial
735 timepoint epifluorescence imaging experiments, number of immune cells on the heart
736 were quantified by manually observing and counting cells moving synchronously with
737 the beating heart. Heart images were acquired using 16X objective. The number of
738 immune cells at the tail were quantified by counting from the caudal end of the vascular
739 loop to the wound edge as performed by others[32,101]. Tail images were acquired using
740 8X objective. CHT and trunk vasculature images were acquired using a 6X objective.
741 Whole larva images were acquired using 2.5X objective.

742

743 **Heart-synchronised light-sheet microscopy**

744

745 Individual larvae were prepared for light sheet fluorescence microscopy (LSFM) by
746 embedding in 1% low melting-point agarose (ThermoFisher) in anesthetized
747 conditioned media inside FEP tubes (Adtech Polymer Engineering). Agar embedding
748 prevents gradual drift of the embryo in the FEP tube, without causing developmental
749 perturbations during long-term imaging. Larvae were used only once for a timelapse
750 imaging experiment, and any repeats shown come from distinct individuals. Larvae
751 were mounted head down such that the heart faces toward both illumination and
752 imaging objectives to improve image clarity. All LSFM experiments were performed at
753 room temperature (23°C). Exposures ranged from 5-15 ms and frequency of scans
754 were 3-5 minutes. Brightfield images acquired at 80 fps were used to inform the optical
755 gating and acquire z slices in a set phase of cardiac contraction, usually mid diastole.
756 The setup of our custom-built LSFM system has been previously reported in detail[38].

757

758 **Metronidazole-nitroreductase macrophage ablation model**

759

760 In order to selectively ablate macrophages prior to cardiac injury, embryos were
761 treated incubated as previously described until 48 hpf and then treated as follows.
762 Embryos were carefully dechorionated at 48 hpf and screened based on fluorescence
763 and split into groups appropriate to the experiment, for example larvae were always
764 split into csf1ra:gal4;UAS:NfsB-mCherry+ and csf1ra:gal4;UAS:NfsB-mCherry-.

765 Embryos were then transferred to either conditioned water or a 0.5mM metronidazole
766 (Thermo Fisher Scientific) solution, both solutions also contained 0.003%
767 phenylthiourea (Thermo Fisher Scientific) and 0.2% DMSO (Sigma Aldrich). Larvae
768 were then incubated in these solutions in the dark at 28. 5°C for 24 hours prior to injury
769 at 72 hpf. Larvae were then removed from the metronidazole solution and vehicle
770 solution and placed in fresh conditioned water + 0.003% phenylthiourea for the
771 remainder of the experiment. As shown in Figure 2 and Supplementary Figure 2, this
772 is sufficient to ablate macrophages prior to injury and completely block subsequent
773 macrophage recruitment to the injured heart.
774
775 **Neutral red staining**
776
777 Larvae were incubated at 72 hpf in 5ug/mL neutral red in conditioned water for 5 hours
778 in the dark at 28.5°C. Larvae were then washed twice for 5 minutes in conditioned
779 water, anaesthetised with 40 µg/ml tricaine methanesulfonate and imaged by
780 brightfield microscopy on a Leica M205 FA stereomicroscope.
781
782 **Genotyping of *irf8-/-* mutants**
783
784 Adult (>30 dpf) zebrafish arising from heterozygous *irf8* mutant incrosses were
785 anaesthetised in 40 µg/ml tricaine methanesulfonate and a lobe of caudal fin removed
786 by scalpel. After clipping, fins were digested to extract DNA using 10mg/ml Prot K,
787 incubated at 65oC for 1 hr. This incubation ends with 15 minutes at 95ºC to denature
788 the Proteinase K. A section of irf8 flanking the mutation locus was then amplified from
789 the extracted DNA by PCR using Forward -ACATAAGGCGTAGAGATTGGACG and
790 Reverse -GAAACATAGTGCGGTCCTCATCC primers and REDTaq® ReadyMix™
791 PCR Reaction Mix. The PCR product was then digested for 30 mins at 37 ºC using
792 AVA1 restriction enzyme (New England Bioscience) and the product run on a 2%
793 agarose gel. WT = AvaI digest site is present = PCR product is cleaved to give two
794 bands with sizes of approximately 200 and 100 bp. irf8 -/- = AvaI digest site is absent
795 due to mutation = PCR product is not cut. A single band is observed with a size of 286
796 bp. irf8 +/- = Three bands as above.
797
798 **Microinjection recombinant proteins and intravital stains**

799

800 Microinjections were performed on larvae at 72 hpf using a Narishige IM-300
801 Microinjector and pulled thin wall glass capillaries (Harvard Apparatus), administered
802 under anaesthesia by intravenous microinjection through the cardiac sinus venosus
803 (SV) that drains the common cardinal vein (CCV). An injection volume of 1 nL was
804 used for all intravenous injections to minimise disruption to blood volume.
805
806 For propidium iodide intravital staining, 1nL 100µg/ml propidium iodide in DPBS was
807 injected immediately following injury at 0.5 hpi. Larvae were then immediately imaged
808 by heart synchronised light-sheet microscopy at 1 hpi. Injection of recombinant zfIFN-
809 γ-rel (IFN-1.1) (Kingfisher Bioscience) was administered as a single 1nL 132nM dose
810 at 72 hpf. Lyophilised IFN- γ-rel was reconstituted in PBS + 0.1% BSA (carrier protein)
811 and PBS + 0.1% BSA was used as the vehicle control solution. Injections of
812 recombinant zfVEGFaa (Kingfisher Bioscience) were administered as single 1nL 0.25
813 ug/ul doses at 72 hpf (protein reconstituted as above).
814
815 **Trunk laser injury and neovascularisation**
816
817 A Zeiss Photo Activated Laser Microdissection (PALM) laser system (Zeiss,
818 Oberkochen, Germany) was used to precisely cause a localised injury to the skeletal
819 muscle segment directly dorsal to the posterior end of the cloaca in anesthetized 72
820 hpf larvae. Care was taken not to damage the intersegmental vessels. Muscle can
821 seen to be successfully injured by disruption of its usually smooth striated appearance
822 via monitoring in brightfield. Additionally, successfully injured larvae will be paralysed
823 for approximately 24 hpi due to the proximity of the spinal cord. Uninjured larvae were
824 treated in the same manner up to the point of laser injury, when they were individually
825 transferred into single wells of a 24-well plate and maintained in the same
826 environmental conditions as injured fish. Larvae were then incubated until 48 hpi
827 28.5°C in conditioned media/water + 0.1% methylene blue + (W/V) 0.003%
828 phenylthiourea (Thermo Fisher Scientific) and imaged at room temperature (23°C)
829 using epifluorescence. At 48 hpi, neovasculature can be visualised by *kdrl:GFP*
830 fluorescence to have invaded the injured skeletal muscle in a portion of injured larvae.
831 The total length of the neovascular network can be quantified post-acquisitionally by
832 image analysis in FIJI (National Institutes of Health).

833

834 **Tail fin transection injury**

835

836 The tail/caudal fin of anesthetized 72 hpf larvae was transected using a sterile scalpel,
837 avoiding damage to the end of the notochord and vasculature and as previously
838 reported[102]. Uninjured (control) fish were treated in the same manner up to the point
839 of transection, when they were separated into a 24-well plate and maintained in the
840 same environmental conditions as injured fish.

841

842 **Histological staining**

843

844 To detect cell death at the injured ventricle, whole-mount larval TUNEL staining was
845 performed. Larvae were fixed in 4% PFA for 30 mins and transferred to 1:10 dilution
846 of PBS. Larvae were subsequently digested in 1 µg/ml Proteinase K for 1 h. Larvae
847 were re-fixed in 4% PFA for 20 mins and subsequently washed in PBT. TUNEL
848 staining was performed using ApopTag Red In situ kit (MilliporeSigma) to label
849 apoptotic cells, as described previously[32]. Stained hearts were imaged using LSFM.

850

851 EdU staining was performed by incubating larvae in 1mM EdU (5-ethynyl-2′-
852 deoxyuridine) (Abcam) in 1 % DMSO (Sigma Aldrich) in conditioned water + 0.003%
853 phenylthiourea (Thermo Fisher Scientific) for 24 hours beginning either at 0 hpi or 24
854 hpi depending on the experiment. Larvae were incubated at 28.5°C in the dark. Larvae
855 were then fixed for 2 hours at room temperature in 4% PFA, permeabilised in
856 permeabilisation solution (PBS-Triton-X 0.1% + 1% Tween + 1% DMSO) and
857 pericardium punctured using a glass microinjection needle (further improving
858 permeability). Larvae were then washed twice in PBS-3% BSA and incubated for 2
859 hours at room temperature in CLICK reaction mixture from Click-iT™ EdU Imaging Kit
860 with Alexa Fluor™ 594 (Invitrogen) made according to manufacturers' instructions.
861 Larvae were finally washed once in PBS-3%BSA and twice in PBS-0.1% tween and
862 imaged by LSFM.

863

864 **Heart lesion size quantification**

865

866 Larval hearts expressing the transgene *myl7:GFP* were imaged by heart-synchronised
867 light-sheet imaging as described above. Exposure was kept consistent at 10ms as well
868 as z slice spacing (1 μm) and heart contraction phase was locked to mid diastole for
869 all larvae. Z stacks were surface rendered in IMARIS (Bitplane) based on absolute
870 intensity and software-suggested segmentation and rendering parameters. Lesion
871 area, visualised as a render-free hole in the myocardium, was then traced around
872 manually and lesion area quantified in FIJI (National Institutes of Health).
873
874 **Ventricular ejection fraction analysis**
875
876 Larval hearts of *Tg(myl7:GFP)* larvae were imaged at 80 fps in brightfield using a Leica
877 M205 FA epifluorescence stereomicroscope to capture when the ventricle was in
878 diastole and systole. The ventricular area in diastole and systole was measured
879 manually in FIJI and ventricular ejection fraction calculated using the formula 100 X
880 [(Diastolic Area – Systolic Area)/Diastolic Area][31]. Ventricular ejection fraction by area
881 was then converted to ejection fraction by volume using the formula 'Ejection fraction
882 by area x 2.33 = Ejection fraction by volume' derived in Supplementary Figure 4. Over
883 the small range of ejection fractions that occur in larval hearts, the relationship can be
884 considered to approximate to a linear one.
885
886 **Quantification of cell number by image analysis**
887
888 To quantify the number of cardiomyocytes in *Tg(myl7:h2b-GFP)* and
889 *Tg(myl7:nlsDsRed)* larval hearts z stacks of hearts acquired by LSFM were imported
890 into FIJI and nuclei counted by the plugin Trackmate. Briefly, key segementation
891 parameters 'Estimated blob diameter'=5.5, 'Threshold'=0.9 were taken as a starting
892 point and optimised manually per experiment until all nuclei are counted successfully.
893 The heart atrium is excluded manually by x coordinate filtering and ventricular
894 cardiomyocytes are then automatically by the plug in.
895
896 In order to automatically quantify the percentage of EdU+ ventricular cardiomyocytes
897 in *Tg(myl7:h2b-GFP)* larval hearts a custom FIJI macro was written to exclude non-
898 cardiomyocyte EdU signal. This is necessary as cardiomyocytes have a much lower
899 turnover rate than surrounding cells in the pericardium, endocardium and blood and

so represent a minority of EdU+ cells. Briefly, the Bersen segmentation method was used to mask areas of GFP fluorescence per z slice and these masks subsequently applied as a crop ROI to EdU signal in the 564 (red) channel of RGB images. Slices were then reassembled and merged into maximum intensity projections where the FIJI Trackmate plugin was used to count both the total number of GFP+ cardiomyocyte nuclei and EdU+ cardiomyocyte nuclei. This quantification then allowed the percentage of EdU+ cardiomycytes to be calculated in an unbiased way per larval heart.

Quantification of notch signalling by image analysis

In order to objectively identify whether the hearts from *Tg(Tp1:venus-PEST)* larvae possessed venus signal in the endocardium above that of background, and were therefore 'notch+', the following approach was used. Treatment groups were blinded to the analyser and z stacks opened in FIJI. The automatic brightness and contrast function was used to objectively enhance the signal in the heart and the clear interface between the granular autofluorescence of the chamber blood and the smooth autofluorescence of the myocardium searched for venus expression. The distinctive morphology and location of endothelium allowed for unambiguous identification of venus+ status.

For the quantification of the total myocardial *Tp:venus-PEST* fluorescence, z stacks were blinded and processed in FIJI. Stacks were converted to maximum intensity projections and a standardised size ROI was manually positioned over the notch^{high} atrioventricular valve allowing it to be cropped out of the image and preventing it from interfering with myocardial signal. This is because during development it exhibits exceptionally high *Tp1:venus-PEST* fluorescence, unlike the endocardium whose fluorescence is negligible relative to the myocardium. Ventricles were then manually traced, avoiding the bulbous arteriosus as it is similarly notch^{high} during development and fluorescence summed. Fluorescence was then normalised by subtracting background fluorescence of venus-negative larvae imaged similarly.

Pharmacological inhibition of larval signalling

934 To inhibit VEGF signalling larvae were bathed in pan-VEGFR antagonist
935 AV951/Tivozanib (Stratech Scientific) 0-48 hpi. AV951 was dissolved in 0.1% DMSO
936 in conditioned water + 0.003% phenylthiourea to make a 10nM solution, with just 0.1%
937 DMSO in conditioned water + 0.003% phenylthiourea becoming the vehicle control. In
938 order to pulse larvae with EdU, the orginal solution was replaced the same solution
939 was except for the addition of 1mM EdU at 1% DMSO.
940
941 To inhibit notch signalling, larvae were bathed in gamma secretase inhibitor DAPT
942 (Cambridge Bioscience) 0-48 hpi. DAPT was dissolved in 0.2% DMSO in conditioned
943 water + 0.003% phenylthiourea to make a 100μM solution, with just 0.2% DMSO in
944 conditioned water + 0.003% phenylthiourea becoming the vehicle control. Note, DAPT
945 must be dissolved in DMSO prior to the addition of water to prevent precipitation.
946
947 In order to inhibit neuregulin-ERBB signalling, the ErBB2 antagonist AG1478 was
948 used. Larvae were bathed in 1.75 μM AG1478 (Cambridge Bioscience) dissolved in
949 0.25% DMSO in conditioned water + 0.003% phenylthiourea over 0-48 hpi.
950
951 **Extraction of larval hearts and RNA extraction**
952
953 Following laser injury at 72 hpf *Tg(myl7:gal4::GFP;UAS:mRFP)* larvae were incubated
954 at 28.5°C in conditioned media/water + 0.1% methylene blue (w/v) + 0.003%
955 phenylthiourea. At 48 hpi uninjured and injured larvae were given an overdose of
956 tricaine at 400 µg/ml, following which hearts were extracted. We adapted the protocol
957 of Burns and MacRae[103] to increase the yield of heart retrieval from ~50% to ~70%.
958 Briefly, ~30 larvae were placed in 2mL eppendorf tubes, the conditioned water drained
959 and replaced with ice cold Leibovitz's L-15 Medium supplemented with 10% FCS. A
960 19-gauge needle coupled to a 5mL syringe was used to shear the larvae by aspiration
961 and therefore dissociate hearts from the rest of the larva. The lysate was then
962 inspected by epifluorescence microscopy and mRFP+ hearts and collected to be kept
963 on ice. Hearts were then digested at for 10 minutes at 4°C in protease solution (5 mM
964 CaCl2,10 mg/ml B. Licheniformis protease, 125 U/mL DNase I in 1x PBS) with
965 occasional aspiration to aid digestion (Truong et al,). RNA was then extracted using a
966 RNeasy Plus Micro Kit (Qiagen) following direct lysis with RLT lysis buffer according

967 to manufacturer's instructions. RNA concentration was measured by Qubit and
968 integrity by Bioanalyser. RIN score for all samples ranged between 9.6-10.
969
970 **RNAseq analysis**
971
972 RNA was sequenced by Genewiz, Leipzig, Germany by Illumina NovaSeq, PE
973 2x150. Genewiz also used eseq2 package was used in R to evaluate sequencing
974 quality, trim reads, map to the *Danio rerio* genome and generate gene counts/hits.
975 Sequence reads were trimmed using Trimmomatic v.0.36. The trimmed reads were
976 mapped to the Danio rerio GRCz10.89 reference genome available on ENSEMBL
977 using the STAR aligner v.2.5.2b. Unique gene hit counts were calculated by using
978 featureCounts from the Subread package v.1.5.2. Only unique reads that fell within
979 exon regions were counted. The Wald test was used to generate p-values and log2
980 fold changes. A gene ontology analysis was performed on the statistically significant
981 set of genes by implementing the software GeneSCF v.1.1-p2. The zfin GO list was
982 used to cluster the set of genes based on their biological processes and determine
983 their statistical significance. The volcano plot was generated by a custom R script
984 and heatmap constructed using the pHeatmap package. For the heatmap z scaled
985 log2(Reads) were clustered via Pearson correlation and clusters thresholded based
986 on the resulting dendrogram. The heatmap was generated using the pHeatmap
987 function in R.
988
989
990
991
992
993 **Statistics**
994
995 Graphs and statistics were curated in GraphPad Prism 9.1 software (GraphPad
996 Software). Data were analyzed by student *t*-test, one-way ANOVA or two-way ANOVA
997 followed by an appropriate multiple comparison *post hoc* test. All statistical tests, *p*-
998 values and *n* numbers used are given in figure legends.
999
1000

Acknowledgments

This work was funded by a British Heart Foundation (BHF) CoRE award (RE/13/3/30183), Medical Research Scotland studentship (PhD-1049-2016), NC3R studentship (NC/P002196/1), BHF New Horizons grant (NH/14/2/31074), and a Medical Research Council UK award (MR/K013386/1). Bioinformatics and RNAseq performed by Genewiz, Leipzig, Germany. We also acknowledge Amelia Edmondson-Stait, University of Edinburgh, for her advice and input on RNAseq analysis.

Author Contributions

FAB conceived of and designed the study. FAB, AK and GM carried out all experiments. Image analysis was performed by FB and AK. LSFM-related technical assistance was provided by JMT. FAB wrote the manuscript. KRS, EGS and MB provided expertise regarding all RNA work. KRS helped optimise larval heart extraction and RNA extraction. JMT, CST, JJM, GM, MB, AGR, and MAD edited the manuscript. MAD, AGR, and CST supervised the study. All authors contributed to the article and approved the submitted version.

References

1. Ohnmacht, J., Yang, Y., Maurer, G. W., Barreiro-Iglesias, A., Tsarouchas, T. M., Wehner, D., Sieger, D., Becker, C. G. & Becker, T. Spinal motor neurons are regenerated after mechanical lesion and genetic ablation in larval zebrafish. *Dev.* **143**, 1464–1474 (2016).
2. Becker, C. G., Lieberoth, B. C., Morellini, F., Feldner, J., Becker, T. & Schachner, M. L1.1 is involved in spinal cord regeneration in adult zebrafish. *J. Neurosci.* **24**, 7837–7842 (2004).
3. Bensimon-Brito, A., Ramkumar, S., Boezio, G. L. M., Guenther, S., Kuenne, C., Helker, C. S. M., Sánchez-Iranzo, H., Iloska, D., Piesker, J., Pullamsetti, S., Mercader, N., Beis, D. & Stainier, D. Y. R. TGF-β Signaling Promotes Tissue Formation during Cardiac Valve Regeneration in Adult Zebrafish. *Dev. Cell* **0**,

1035 (2019).
1036 4. Sander, V., Davidson, A. J., Sander, V. & Davidson, A. J. Kidney Injury and
1037 Regeneration in Zebrafish. *Semin. Nephrol.* **34**, 437–444 (2014).
1038 5. Basu Mallik, S., Jayashree, B. S. & Shenoy, R. R. Epigenetic modulation of
1039 macrophage polarization- perspectives in diabetic wounds. *J. Diabetes*
1040 *Complications* **0**, (2018).
1041 6. González-Rosa, J. M., Martín, V., Peralta, M., Torres, M. & Mercader, N.
1042 Extensive scar formation and regression during heart regeneration after
1043 cryoinjury in zebrafish. *Development* **138**, 1663–1674 (2011).
1044 7. Leuschner, F., Rauch, P. J., Ueno, T., Gorbatov, R., Marinelli, B., Lee, W. W.,
1045 Dutta, P., Wei, Y., Robbins, C., Iwamoto, Y., Sena, B., Chudnovskiy, A.,
1046 Panizzi, P., Keliher, E., Higgins, J. M., Libby, P., Moskowitz, M. A., Pittet, M. J.,
1047 Swirski, F. K., Weissleder, R. & Nahrendorf, M. Rapid monocyte kinetics in
1048 acute myocardial infarction are sustained by extramedullary monocytopoiesis.
1049 *J. Exp. Med.* **209**, 123–37 (2012).
1050 8. Murry, C. E., Reinecke, H. & Pabon, L. M. Regeneration Gaps. Observations
1051 on Stem Cells and Cardiac Repair. *Journal of the American College of*
1052 *Cardiology* vol. 47 1777–1785 (2006).
1053 9. Bergmann, O., Zdunek, S., Felker, A., Salehpour, M., Alkass, K., Bernard, S.,
1054 Sjostrom, S. L., Szewczykowska, M., Jackowska, T., dos Remedios, C., Malm,
1055 T., Andrä, M., Jashari, R., Nyengaard, J. R., Possnert, G., Jovinge, S., Druid,
1056 H. & Frisén, J. Dynamics of Cell Generation and Turnover in the Human Heart.
1057 *Cell* **161**, 1566–1575 (2015).
1058 10. Pfeffer, M. A. & Braunwald, E. Ventricular remodeling after myocardial
1059 infarction. Experimental observations and clinical implications. *Circulation* **81**,
1060 1161–72 (1990).
1061 11. Richardson, W. J., Clarke, S. A., Quinn, T. A. & Holmes, J. W. Physiological
1062 Implications of Myocardial Scar Structure. *Compr. Physiol.* **5**, 1877–909
1063 (2015).
1064 12. Jopling, C., Sleep, E., Raya, M., Martí, M., Raya, A. & Belmonte, J. C. I.
1065 Zebrafish heart regeneration occurs by cardiomyocyte dedifferentiation and
1066 proliferation. *Nature* **464**, 606–609 (2010).
1067 13. Kikuchi, K., Holdway, J. E., Werdich, A. A., Anderson, R. M., Fang, Y.,
1068 Egnaczyk, G. F., Evans, T., MacRae, C. A., Stainier, D. Y. R. & Poss, K. D.

1069 Primary contribution to zebrafish heart regeneration by gata4+
1070 cardiomyocytes. *Nature* **464**, 601–605 (2010).
1071 14. González-rosa, J. M., Martín, V., Peralta, M., Torres, M. & Mercader, N.
1072 Extensive scar formation and regression during heart regeneration after
1073 cryoinjury in zebrafish. **1674**, 1663–1674 (2011).
1074 15. Aurora, A. B., Porrello, E. R., Tan, W., Mahmoud, A. I., Hill, J. A., Bassel-duby,
1075 R., Sadek, H. A. & Olson, E. N. Macrophages are required for neonatal heart
1076 regeneration. **124**, (2014).
1077 16. Godwin, J. W., Debuque, R., Salimova, E. & Rosenthal, N. A. Heart
1078 regeneration in the salamander relies on macrophage-mediated control of
1079 fibroblast activation and the extracellular landscape. *npj Regen. Med.* **2**, 22
1080 (2017).
1081 17. Lai, S.-L., Marín-Juez, R., Moura, P. L., Kuenne, C., Lai, J. K. H., Tsedeke, A.
1082 T., Guenther, S., Looso, M. & Stainier, D. Y. Reciprocal analyses in zebrafish
1083 and medaka reveal that harnessing the immune response promotes cardiac
1084 regeneration. *Elife* **6**, (2017).
1085 18. Tsarouchas, T. M., Wehner, D., Cavone, L., Munir, T., Keatinge, M.,
1086 Lambertus, M., Underhill, A., Barrett, T., Kassapis, E., Ogryzko, N., Feng, Y.,
1087 van Ham, T. J., Becker, T. & Becker, C. G. Dynamic control of proinflammatory
1088 cytokines Il-1β and Tnf-α by macrophages in zebrafish spinal cord
1089 regeneration. *Nat. Commun.* **9**, 4670 (2018).
1090 19. Carrillo, S. A., Anguita-Salinas, C., Peña, O. A., Morales, R. A., Muñoz-
1091 Sánchez, S., Muñoz-Montecinos, C., Paredes-Zúñiga, S., Tapia, K. & Allende,
1092 M. L. Macrophage Recruitment Contributes to Regeneration of
1093 Mechanosensory Hair Cells in the Zebrafish Lateral Line. *J. Cell. Biochem.*
1094 **117**, 1880–1889 (2016).
1095 20. Puranik, A. S., Leaf, I. A., Jensen, M. A., Hedayat, A. F., Saad, A., Kim, K.-W.,
1096 Saadalla, A. M., Woollard, J. R., Kashyap, S., Textor, S. C., Grande, J. P.,
1097 Lerman, A., Simari, R. D., Randolph, G. J., Duffield, J. S. & Lerman, L. O.
1098 Kidney-resident macrophages promote a proangiogenic environment in the
1099 normal and chronically ischemic mouse kidney. *Sci. Rep.* **8**, 13948 (2018).
1100 21. Gurevich, D. B., Severn, C. E., Twomey, C., Greenhough, A., Cash, J., Toye,
1101 A. M., Mellor, H. & Martin, P. Live imaging of wound angiogenesis reveals
1102 macrophage orchestrated vessel sprouting and regression. *EMBO J.* **37**,

1103 e97786 (2018).
1104 22. Herzog, C., Pons Garcia, L., Keatinge, M., Greenald, D., Moritz, C., Peri, F. &
1105 Herrgen, L. Rapid clearance of cellular debris by microglia limits secondary
1106 neuronal cell death after brain injury in vivo. *Development* **146**, dev174698
1107 (2019).
1108 23. Nahrendorf, M., Swirski, F. K., Aikawa, E., Stangenberg, L., Wurdinger, T.,
1109 Figueiredo, J.-L., Libby, P., Weissleder, R. & Pittet, M. J. The healing
1110 myocardium sequentially mobilizes two monocyte subsets with divergent and
1111 complementary functions. *J. Exp. Med.* **204**, 3037–3047 (2007).
1112 24. Sager, H. B., Hulsmans, M., Lavine, K. J., Moreira, M. B., Heidt, T., Courties,
1113 G., Sun, Y., Iwamoto, Y., Tricot, B., Khan, O. F., Dahlman, J. E., Borodovsky,
1114 A., Fitzgerald, K., Anderson, D. G., Weissleder, R., Libby, P., Swirski, F. K. &
1115 Nahrendorf, M. Proliferation and Recruitment Contribute to Myocardial
1116 Macrophage Expansion in Chronic Heart Failure. *Circ. Res.* **119**, 853–64
1117 (2016).
1118 25. Panizzi, P., Swirski, F. K., Figueiredo, J. L., Waterman, P., Sosnovik, D. E.,
1119 Aikawa, E., Libby, P., Pittet, M., Weissleder, R. & Nahrendorf, M. Impaired
1120 Infarct Healing in Atherosclerotic Mice With Ly-6Chi Monocytosis. *J. Am. Coll.*
1121 *Cardiol.* **55**, 1629–1638 (2010).
1122 26. Nahrendorf, M. & Swirski, F. K. Monocyte and Macrophage Heterogeneity in
1123 the Heart. **02114**, 1624–1634 (2013).
1124 27. Lavin, Y., Winter, D., Blecher-Gonen, R., David, E., Keren-Shaul, H., Merad,
1125 M., Jung, S. & Amit, I. Tissue-Resident Macrophage Enhancer Landscapes
1126 Are Shaped by the Local Microenvironment. *Cell* **159**, 1312–1326 (2014).
1127 28. Xue, J., Schmidt, S. V, Sander, J., Draffehn, A., Krebs, W., Quester, I., Nardo,
1128 D. De, Gohel, T. D., Emde, M., Schmidleithner, L., Ganesan, H., Nino-castro,
1129 A., Mallmann, M. R., Labzin, L., Theis, H., Kraut, M., Beyer, M., Latz, E.,
1130 Freeman, T. C., Ulas, T. & Schultze, J. L. Resource Transcriptome-Based
1131 Network Analysis Reveals a Spectrum Model of Human Macrophage
1132 Activation. *Immunity* **40**, 274–288 (2014).
1133 29. Sanz-Morejón, A., García-Redondo, A. B., Reuter, H., Marques, I. J., Bates,
1134 T., Galardi-Castilla, M., Große, A., Manig, S., Langa, X., Ernst, A., Piragyte, I.,
1135 Botos, M.-A., González-Rosa, J. M., Ruiz-Ortega, M., Briones, A. M., Salaices,
1136 M., Englert, C. & Mercader, N. Wilms Tumor 1b Expression Defines a Pro-

1137 regenerative Macrophage Subtype and Is Required for Organ Regeneration in
1138 the Zebrafish. *Cell Rep.* **28**, 1296-1306.e6 (2019).
1139 30. Nguyen-Chi, M., , B´eryl Laplace-BuilheTravnickova, J., Luz-crawford, P.,
1140 Tejedor, G., Phan, Q. T., Duroux-richard, I., Levraud, J., Kissa, K., Lutfalla, G.,
1141 Jorgensen, C., Djouad, F., Laplace-Builhe, B., Travnickova, J., Luz-crawford,
1142 P., Tejedor, G., Phan, Q. T., Duroux-richard, I., Levraud, J., Kissa, K., Lutfalla,
1143 G., Jorgensen, C. & Djouad, F. Identification of polarized macrophage subsets
1144 in zebrafish. *Elife* **4**, 1–14 (2015).
1145 31. Matrone, G., Taylor, J., Wilson, K., … J. B.-I. journal of & 2013, undefined.
1146 Laser-targeted ablation of the zebrafish embryonic ventricle: a novel model of
1147 cardiac injury and repair. *Elsevier*.
1148 32. Kaveh, A., Bruton, F. A., Buckley, C., Oremek, M. E. M., Tucker, C. S., Mullins,
1149 J. J., Taylor, J. M., Rossi, A. G. & Denvir, M. A. Live Imaging of Heart Injury in
1150 Larval Zebrafish Reveals a Multi-Stage Model of Neutrophil and Macrophage
1151 Migration. *Front. Cell Dev. Biol.* **8**, 579943 (2020).
1152 33. Shiau, C. E., Kaufman, Z., Meireles, A. M. & Talbot, W. S. Differential
1153 Requirement for irf8 in Formation of Embryonic and Adult Macrophages in
1154 Zebrafish. *PLoS One* **10**, 1–15 (2015).
1155 34. Bevan, L., Lim, Z. W., Venkatesh, B., Riley, P. R., Martin, P. & Richardson, R.
1156 J. Specific macrophage populations promote both cardiac scar deposition and
1157 subsequent resolution in adult zebrafish. *Cardiovasc. Res.* (2019)
1158 doi:10.1093/cvr/cvz221.
1159 35. Pisharath, H., Rhee, J. M., Swanson, M. A., Leach, S. D. & Parsons, M. J.
1160 Targeted ablation of beta cells in the embryonic zebrafish pancreas using E.
1161 coli nitroreductase. *Mech. Dev.* **124**, 218–229 (2007).
1162 36. Yoshimura, C., Nagasaka, A., Kurose, H. & Nakaya, M. Efferocytosis during
1163 myocardial infarction. *J. Biochem.* **168**, 1–6 (2020).
1164 37. Chablais, F., Veit, J., Rainer, G. & Jaźwińska, A. The zebrafish heart
1165 regenerates after cryoinjury-induced myocardial infarction. *BMC Dev. Biol.* **11**,
1166 21 (2011).
1167 38. Taylor, J. M., Nelson, C. J., Bruton, F. A., Baghbadrani, A. K., Buckley, C.,
1168 Tucker, C. S., Rossi, A. G., Mullins, J. J. & Denvir, M. A. Adaptive prospective
1169 optical gating enables day-long 3D time-lapse imaging of the beating
1170 embryonic zebrafish heart. *Nat. Commun.* **10**, 1–15 (2019).

1171 39. Bajpai, G., Schneider, C., Wong, N., Bredemeyer, A., Hulsmans, M.,
1172 Nahrendorf, M., Epelman, S., Kreisel, D., Liu, Y., Itoh, A., Shankar, T. S.,
1173 Selzman, C. H., Drakos, S. G. & Lavine, K. J. The human heart contains
1174 distinct macrophage subsets with divergent origins and functions. *Nat. Med.*
1175 **24**, 1234–1245 (2018).
1176 40. Lavine, K. J., Epelman, S., Uchida, K., Weber, K. J., Nichols, C. G., Schilling,
1177 J. D., David, M., Randolph, G. J., Mann, D. L., Lavine, K. J., Epelman, S.,
1178 Uchida, K., Weber, K. J., Nichols, C. G. & Schilling, J. D. Distinct macrophage
1179 lineages contribute to disparate patterns of cardiac recovery and remodeling in
1180 the neonatal and adult heart. **113**, (2016).
1181 41. Karra, R., Foglia, M. J., Choi, W.-Y., Belliveau, C., DeBenedittis, P. & Poss, K.
1182 D. Vegfaa instructs cardiac muscle hyperplasia in adult zebrafish. *Proc. Natl.*
1183 *Acad. Sci. U. S. A.* 201722594 (2018) doi:10.1073/pnas.1722594115.
1184 42. Zentilin, L., Puligadda, U., Lionetti, V., Zacchigna, S., Collesi, C., Pattarini, L.,
1185 Ruozi, G., Camporesi, S., Sinagra, G., Pepe, M., Recchia, F. A. & Giacca, M.
1186 Cardiomyocyte VEGFR-1 activation by VEGF-B induces compensatory
1187 hypertrophy and preserves cardiac function after myocardial infarction. *FASEB*
1188 *J. • Res. Commun. FASEB J* **24**, 1467–1478 (2010).
1189 43. Kivelä, R., Hemanthakumar, K. A., Vaparanta, K., Robciuc, M., Izumiya, Y.,
1190 Kidoya, H., Takakura, N., Peng, X., Sawyer, D. B., Elenius, K., Walsh, K. &
1191 Alitalo, K. Endothelial Cells Regulate Physiological Cardiomyocyte Growth via
1192 VEGFR2-Mediated Paracrine Signaling. *Circulation* **139**, 2570–2584 (2019).
1193 44. Chimote, G., Sreenivasan, J., Pawar, N., Subramanian, J., Sivaramakrishnan,
1194 H. & Sharma, S. Comparison of effects of anti-angiogenic agents in the
1195 zebrafish efficacy-toxicity model for translational anti-angiogenic drug
1196 discovery. *Drug Des. Devel. Ther.* **8**, 1107–1123 (2014).
1197 45. Kugler, E. C., Lessen, M., Daetwyler, S., Chhabria, K., Savage, A. M., Silva,
1198 V., Plant, K., MacDonald, R. B., Huisken, J., Wilkinson, R. N., Schulte-Merker,
1199 S., Armitage, P. & Chico, T. J. Cerebrovascular endothelial cells form transient
1200 Notch-dependent cystic structures in zebrafish. *EMBO Rep.* **20**, (2019).
1201 46. Zhao, L., Borikova, A. L., Ben-Yair, R., Guner-Ataman, B., MacRae, C. A., Lee,
1202 R. T., Geoffrey Burns, C. & Burns, C. E. Notch signaling regulates
1203 cardiomyocyte proliferation during zebrafish heart regeneration. *Proc. Natl.*
1204 *Acad. Sci. U. S. A.* **111**, 1403–1408 (2014).

1205 47. Raya, A., Koth, C. M., Büscher, D., Kawakami, Y., Itoh, T., Raya, R. M.,
1206 Sternik, G., Tsai, H.-J., Rodríguez-Esteban, C. & Izpisúa-Belmonte, J. C.
1207 Activation of Notch signaling pathway precedes heart regeneration in
1208 zebrafish. *Proc. Natl. Acad. Sci. U. S. A.* **100 Suppl 1**, 11889–95 (2003).
1209 48. Zhao, L., Ben-Yair, R., Burns, C. G. E. G. & Burns, C. G. E. G. Endocardial
1210 Notch Signaling Promotes Cardiomyocyte Proliferation in the Regenerating
1211 Zebrafish Heart through Wnt Pathway Antagonism. *Cell Rep.* **26**, 546-554.e5
1212 (2019).
1213 49. Samsa, L. A., Givens, C., Tzima, E., Stainier, D. Y. R., Qian, L. & Liu, J.
1214 Cardiac contraction activates endocardial Notch signaling to modulate
1215 chamber maturation in zebrafish. *Development* **142**, 4080–4091 (2015).
1216 50. Gemberling, M., Karra, R., Dickson, A. L. & Poss, K. D. Nrg1 is an injury-
1217 induced cardiomyocyte mitogen for the endogenous heart regeneration
1218 program in zebrafish. 1–17 (2015) doi:10.7554/eLife.05871.
1219 51. Bersell, K., Arab, S., Haring, B. & Kühn, B. Neuregulin1/ErbB4 Signaling
1220 Induces Cardiomyocyte Proliferation and Repair of Heart Injury. *Cell* **138**, 257–
1221 270 (2009).
1222 52. Honkoop, H., Bakker, D. E. de, Aharonov, A., Kruse, F., Shakked, A., Nguyen,
1223 P. D., Heus, C. de, Garric, L., Muraro, M. J., Shoffner, A., Tessadori, F.,
1224 Peterson, J. C., Noort, W., Bertozzi, A., Weidinger, G., Posthuma, G., Grün,
1225 D., Laarse, W. J. van der, Klumperman, J., Jaspers, R. T., Poss, K. D.,
1226 Oudenaarden, A. van, Tzahor, E., Bakkers, J., de Bakker, D. E., Aharonov, A.,
1227 Kruse, F., Shakked, A., Nguyen, P. D., de Heus, C., Garric, L., Muraro, M. J.,
1228 Shoffner, A., Tessadori, F., Peterson, J. C., Noort, W., Bertozzi, A., Weidinger,
1229 G., Posthuma, G., Grun, D., van der Laarse, W. J., Klumperman, J., Jaspers,
1230 R. T., Poss, K. D., van Oudenaarden, A., Tzahor, E. & Bakkers, J. Single-cell
1231 analysis uncovers that metabolic reprogramming by ErbB2 signaling is
1232 essential for cardiomyocyte proliferation in the regenerating heart. *Elife* **8**,
1233 (2019).
1234 53. Rasouli, S. J. & Stainier, D. Y. R. Regulation of cardiomyocyte behavior in
1235 zebrafish trabeculation by Neuregulin 2a signaling. *Nat. Commun.* **8**, 15281
1236 (2017).
1237 54. Uribe, V., Ramadass, R., Dogra, D., Rasouli, S. J., Gunawan, F., Nakajima, H.,
1238 Chiba, A., Reischauer, S., Mochizuki, N. & Stainier, D. Y. R. In vivo analysis of

1239 cardiomyocyte proliferation during trabeculation. (2018)
1240 doi:10.1242/dev.164194.
1241 55. Dovey, H. F., John, V., Anderson, J. P., Chen, L. Z., De Saint Andrieu, P.,
1242 Fang, L. Y., Freedman, S. B., Folmer, B., Goldbach, E., Holsztynska, E. J., Hu,
1243 K. L., Johnson-Wood, K. L., Kennedy, S. L., Kholodenko, D., Knops, J. E.,
1244 Latimer, L. H., Lee, M., Liao, Z., Lieberburg, I. M., Motter, R. N., Mutter, L. C.,
1245 Nietz, J., Quinn, K. P., Sacchi, K. L., Seubert, P. A., Shopp, G. M., Thorsett, E.
1246 D., Tung, J. S., Wu, J., Yang, S., Yin, C. T., Schenk, D. B., May, P. C., Altstiel,
1247 L. D., Bender, M. H., Boggs, L. N., Britton, T. C., Clemens, J. C., Czilli, D. L.,
1248 Dieckman-McGinty, D. K., Droste, J. J., Fuson, K. S., Gitter, B. D., Hyslop, P.
1249 A., Johnstone, E. M., Li, W. Y., Little, S. P., Mabry, T. E., Miller, F. D., Ni, B.,
1250 Nissen, J. S., Porter, W. J., Potts, B. D., Reel, J. K., Stephenson, D., Su, Y.,
1251 Shipley, L. A., Whitesitt, C. A., Yin, T. & Audia, J. E. Functional gamma-
1252 secretase inhibitors reduce beta-amyloid peptide levels in brain. *J.*
1253 *Neurochem.* **76**, 173–181 (2001).
1254 56. Micchelli, C. A., Esler, W. P., Kimberly, W. T., Jack, C., Berezovska, O.,
1255 Kornilova, A., Hyman, B. T., Perrimon, N. & Wolfe, M. S. Gamma-
1256 secretase/presenilin inhibitors for Alzheimer's disease phenocopy Notch
1257 mutations in Drosophila. *FASEB J.* **17**, 79–81 (2003).
1258 57. Geling, A., Steiner, H., Willem, M., Bally-Cuif, L. & Haass, C. A γ-secretase
1259 inhibitor blocks Notch signaling in vivo and causes a severe neurogenic
1260 phenotype in zebrafish. *EMBO Rep.* **3**, 688–694 (2002).
1261 58. Gemberling, M., Karra, R., Dickson, A. L. & Poss, K. D. Nrg1 is an injury-
1262 induced cardiomyocyte mitogen for the endogenous heart regeneration
1263 program in zebrafish. *Elife* **4**, (2015).
1264 59. Han, Y., Chen, A., Umansky, K.-B., Oonk, K. A., Choi, W.-Y., Dickson, A. L.,
1265 Ou, J., Cigliola, V., Yifa, O., Cao, J., Tornini, V. A., Cox, B. D., Tzahor, E. &
1266 Poss, K. D. Vitamin D Stimulates Cardiomyocyte Proliferation and Controls
1267 Organ Size and Regeneration in Zebrafish. *Dev. Cell* **0**, (2019).
1268 60. Vedula, V., Lee, J., Xu, H., Kuo, C. J., Hsiai, T. K. & Marsden, A. L. A method
1269 to quantify mechanobiologic forces during zebrafish cardiac development
1270 using 4-D light sheet imaging and computational modeling. 1–24 (2017).
1271 61. Zuppo, D. A. & Tsang, M. Zebrafish heart regeneration: Factors that stimulate
1272 cardiomyocyte proliferation. *Semin. Cell Dev. Biol.* (2019)

1273 doi:10.1016/J.SEMCDB.2019.09.005.
1274 62. Lyons, D. A., Pogoda, H. M., Voas, M. G., Woods, I. G., Diamond, B., Nix, R.,
1275 Arana, N., Jacobs, J. & Talbot, W. S. erbb3 and erbb2 are essential for
1276 Schwann cell migration and myelination in zebrafish. *Curr. Biol.* **15**, 513–524
1277 (2005).
1278 63. Priya, R., Allanki, S., Gentile, A., Mansingh, S., Uribe, V., Maischein, H. M. &
1279 Stainier, D. Y. R. Tension heterogeneity directs form and fate to pattern the
1280 myocardial wall. *Nature* **588**, 130–134 (2020).
1281 64. Gálvez-Santisteban, M., Chen, D., Zhang, R., Serrano, R., Nguyen, C., Zhao,
1282 L., Nerb, L., Masutani, E. M., Vermot, J., Burns, C. G., Burns, C. E., del Álamo,
1283 J. C. & Chi, N. C. Hemodynamic-mediated endocardial signaling controls in
1284 vivo myocardial reprogramming. *Elife* **8**, (2019).
1285 65. Nguyen-Chi, M., Laplace-builhé, B., Travnickova, J., Luz-crawford, P., Tejedor,
1286 G., Lutfalla, G., Kissa, K., Jorgensen, C. & Djouad, F. TNF signaling and
1287 macrophages govern fin regeneration in zebrafish larvae. *Nat. Publ. Gr.* **8**,
1288 e2979–e2979 (2017).
1289 66. Kuil, L. E., Oosterhof, N., Ferrero, G., Mikulášová, T., Hason, M., Dekker, J.,
1290 Rovira, M., van der Linde, H. C., van Strien, P. M. H., de Pater, E., Schaaf, G.,
1291 Bindels, E. M. J., Wittamer, V. & van Ham, T. J. Zebrafish macrophage
1292 developmental arrest underlies depletion of microglia and reveals Csf1r-
1293 independent metaphocytes. *Elife* **9**, (2020).
1294 67. Lin, X., Zhou, Q., Zhao, C., Lin, G., Xu, J. & Wen, Z. An Ectoderm-Derived
1295 Myeloid-like Cell Population Functions as Antigen Transporters for Langerhans
1296 Cells in Zebrafish Epidermis. *Dev. Cell* **49**, 605-617.e5 (2019).
1297 68. Ginhoux, F., Schultze, J. L., Murray, P. J., Ochando, J. & Biswas, S. K.
1298 perspective New insights into the multidimensional concept of macrophage
1299 ontogeny , activation and function. **17**, (2016).
1300 69. Koth, J., Wang, X., Killen, A. C., Stockdale, W. T., Potts, H. G., Jefferson, A.,
1301 Bonkhofer, F., Riley, P. R., Patient, R. K., Göttgens, B. & Mommersteeg, M. T.
1302 M. Runx1 promotes scar deposition and inhibits myocardial proliferation and
1303 survival during zebrafish heart regeneration. *Development* **147**, (2020).
1304 70. Herrgen, L., Voss, O. P. & Akerman, C. J. Calcium-Dependent Neuroepithelial
1305 Contractions Expel Damaged Cells from the Developing Brain. *Dev. Cell* **31**,
1306 599–613 (2014).

1307 71. Hill, R. A., Damisah, E. C., Chen, F., Kwan, A. C. & Grutzendler, J. Targeted
1308 two-photon chemical apoptotic ablation of defined cell types in vivo. *Nat.*
1309 *Commun.* **8**, 1–15 (2017).
1310 72. van Amerongen, M. J., Harmsen, M. C., van Rooijen, N., Petersen, A. H. & van
1311 Luyn, M. J. A. Macrophage depletion impairs wound healing and increases left
1312 ventricular remodeling after myocardial injury in mice. *Am. J. Pathol.* **170**, 818–
1313 29 (2007).
1314 73. Frantz, S., Hofmann, U., Fraccarollo, D., Schafer, A., Kranepuhl, S., Hagedorn,
1315 I., Nieswandt, B., Nahrendorf, M., Wagner, H., Bayer, B., Pachel, C., Schon,
1316 M. P., Kneitz, S., Bobinger, T., Weidemann, F., Ertl, G., Bauersachs, J.,
1317 Schäfer, A., Kranepuhl, S., Hagedorn, I., Nieswandt, B., Nahrendorf, M.,
1318 Wagner, H., Bayer, B., Pachel, C., Schön, M. P., Kneitz, S., Bobinger, T.,
1319 Weidemann, F., Ertl, G., Bauersachs, J., Schafer, A., Kranepuhl, S.,
1320 Hagedorn, I., Nieswandt, B., Nahrendorf, M., Wagner, H., Bayer, B., Pachel,
1321 C., Schon, M. P., Kneitz, S., Bobinger, T., Weidemann, F., Ertl, G. &
1322 Bauersachs, J. Monocytes/macrophages prevent healing defects and left
1323 ventricular thrombus formation after myocardial infarction. *FASEB J.* **27**, 871–
1324 881 (2013).
1325 74. Leor, J., Palevski, D., Amit, U. & Konfino, T. Seminars in Cell & Developmental
1326 Biology Macrophages and regeneration : Lessons from the heart. *Semin. Cell*
1327 *Dev. Biol.* **58**, 26–33 (2016).
1328 75. Beisaw, A., Kuenne, C., Günther, S., Dallmann, J., Wu, C.-C., Bentsen, M.,
1329 Looso, M. & Stainier, D. AP-1 Contributes to Chromatin Accessibility to
1330 Promote Sarcomere Disassembly and Cardiomyocyte Protrusion during
1331 Zebrafish Heart Regeneration. *Circ. Res.* CIRCRESAHA.119.316167 (2020)
1332 doi:10.1161/CIRCRESAHA.119.316167.
1333 76. Morikawa, Y., Zhang, M., Heallen, T., Leach, J., Tao, G., Xiao, Y., Bai, Y., Li,
1334 W., Willerson, J. T. & Martin, J. F. Actin cytoskeletal remodeling with protrusion
1335 formation is essential for heart regeneration in Hippo-deficient mice. *Sci.*
1336 *Signal.* **8**, (2015).
1337 77. Itou, J., Oishi, I., Kawakami, H., Glass, T. J., Richter, J., Johnson, A., Lund, T.
1338 C. & Kawakami, Y. Migration of cardiomyocytes is essential for heart
1339 regeneration in zebrafish. *Dev.* **139**, 4133–4142 (2012).
1340 78. de Preux Charles, A.-S., Bise, T., Baier, F., Marro, J. & Jaźwińska, A. Distinct

1341 effects of inflammation on preconditioning and regeneration of the adult
1342 zebrafish heart. *Open Biol.* **6**, 160102 (2016).
1343 79. Godwin, J. W., Debuque, R., Salimova, E. & Rosenthal, N. A. Heart
1344 regeneration in the salamander relies on macrophage- mediated control of fi
1345 broblast activation and the extracellular landscape. *npj Regen. Med.* 1–11
1346 (2017) doi:10.1038/s41536-017-0027-y.
1347 80. Marín-juez, R., Marass, M., Gauvrit, S., Rossi, A., Lai, S. & Materna, S. C. Fast
1348 revascularization of the injured area is essential to support zebrafish heart
1349 regeneration. **113**, (2016).
1350 81. Weinberger, M., Simões, F. C., Patient, R., Sauka-Spengler, T. & Riley, P. R.
1351 Functional Heterogeneity within the Developing Zebrafish Epicardium. *Dev.*
1352 *Cell* **0**, (2020).
1353 82. Stevens, S. M., von Gise, A., VanDusen, N., Zhou, B. & Pu, W. T. Epicardium
1354 is required for cardiac seeding by yolk sac macrophages, precursors of
1355 resident macrophages of the adult heart. *Dev. Biol.* **413**, 153–159 (2016).
1356 83. Deniset, J. F., Belke, D., Lee, W.-Y., Weber, G. F., Fedak, P. W. M. & Kubes,
1357 P. Gata6+ Pericardial Cavity Macrophages Relocate to the Injured Heart and
1358 Prevent Cardiac Fibrosis. *Immunity* **51**, 131-140.e5 (2019).
1359 84. Kimmel, C. B., Ballard, W. W., Kimmel, S. R., Ullmann, B. & Schilling, T. F.
1360 Stages of Embryonic Development of the Zebrafish. **10**, (1995).
1361 85. Huang, C. J., Tu, C. T., Hsiao, C. Der, Hsieh, F. J. & Tsai, H. J. Germ-line
1362 transmission of a myocardium-specific GFP transgene reveals critical
1363 regulatory elements in the cardiac myosin light chain 2 promoter of zebrafish.
1364 *Dev. Dyn.* **228**, 30–40 (2003).
1365 86. Yoo, S. K., Deng, Q., Cavnar, P. J., Wu, Y. I., Hahn, K. M. & Huttenlocher, A.
1366 Differential Regulation of Protrusion and Polarity by PI(3)K during Neutrophil
1367 Motility in Live Zebrafish. *Dev. Cell* **18**, 226–236 (2010).
1368 87. Ellett, F., Pase, L., Hayman, J. W., Andrianopoulos, A. & Lieschke, G. J.
1369 mpeg1 promoter transgenes direct macrophage-lineage expression in
1370 zebrafish. *Blood* **117**, e49 (2011).
1371 88. Renshaw, S. A., Loynes, C. A., Trushell, D. M. I., Elworthy, S., Ingham, P. W.
1372 & Whyte, M. K. B. A transgenic zebrafish model of neutrophilic inflammation.
1373 *Blood* **108**, 3976–3978 (2006).
1374 89. Mickoleit, M., Schmid, B., Weber, M., Fahrbach, F. O., Hombach, S.,

1375 Reischauer, S. & Huisken, J. High-resolution reconstruction of the beating
1376 zebrafish heart. *Nat. Methods* **11**, 919–922 (2014).
1377 90. Lin, Y.-F., Swinburne, I. & Yelon, D. Multiple influences of blood flow on
1378 cardiomyocyte hypertrophy in the embryonic zebrafish heart. *Dev. Biol.* **362**,
1379 242–253 (2012).
1380 91. Gray, C., Loynes, C. A., Whyte, M. K. B., Crossman, D. C., Renshaw, S. A. &
1381 Chico, T. J. A. Simultaneous intravital imaging of macrophage and neutrophil
1382 behaviour during inflammation using a novel transgenic zebrafish. 811–819
1383 (2011) doi:10.1160/TH10-08-0525.
1384 92. Davison, J. M., Akitake, C. M., Goll, M. G., Rhee, J. M., Gosse, N., Baier, H.,
1385 Halpern, M. E., Leach, S. D. & Parsons, M. J. Transactivation from Gal4-VP16
1386 transgenic insertions for tissue-specific cell labeling and ablation in zebrafish.
1387 *Dev. Biol.* **304**, 811–824 (2007).
1388 93. Rottbauer, W., Saurin, A. J., Lickert, H., Shen, X., Burns, C. G., Wo, Z. G.,
1389 Kemler, R., Kingston, R., Wu, C. & Fishman, M. Reptin and pontin
1390 antagonistically regulate heart growth in zebrafish embryos. *Cell* **111**, 661–672
1391 (2002).
1392 94. Ninov, N., Borius, M. & Stainier, D. Y. R. Different levels of Notch signaling
1393 regulate quiescence, renewal and differentiation in pancreatic endocrine
1394 progenitors. *Development* **139**, 1557–1567 (2012).
1395 95. Chi, N. C., Shaw, R. M., De Val, S., Kang, G., Jan, L. Y., Black, B. L. &
1396 Stainier, D. Y. R. Foxn4 directly regulates tbx2b expression and
1397 atrioventricular canal formation. *Genes Dev.* **22**, 734–739 (2008).
1398 96. Choi, J., Dong, L., Ahn, J., Dao, D., Hammerschmidt, M. & Chen, J. N. FoxH1
1399 negatively modulates flk1 gene expression and vascular formation in zebrafish.
1400 *Dev. Biol.* **304**, 735–744 (2007).
1401 97. Kikuchi, K., Gupta, V., Wang, J., Holdway, J. E., Wills, A. A., Fang, Y. & Poss,
1402 K. D. tcf21+ epicardial cells adopt non-myocardial fates during zebrafish heart
1403 development and regeneration. *Development* **138**, 2895–902 (2011).
1404 98. Mickoleit, M., Schmid, B., Weber, M., Fahrbach, F. O., Hombach, S.,
1405 Reischauer, S. & Huisken, J. High-resolution reconstruction of the beating
1406 zebrafish heart. *Nat. Methods* **11**, 919–922 (2014).
1407 99. Almeida, R. G., Pan, S., Cole, K. L. H., Williamson, J. M., Early, J. J., Czopka,
1408 T., Klingseisen, A., Chan, J. R. & Lyons, D. A. Myelination of Neuronal Cell

1409 Bodies when Myelin Supply Exceeds Axonal Demand. *Curr. Biol.* **28**, 1296-
1410 1305.e5 (2018).
1411 100. Karlsson, J., Von Hofsten, J. & Olsson, P. E. Generating transparent zebrafish:
1412 A refined method to improve detection of gene expression during embryonic
1413 development. *Mar. Biotechnol.* **3**, 522–527 (2001).
1414 101. Miskolci, V., Squirrell, J., Rindy, J., Vincent, W., Sauer, J. D., Gibson, A.,
1415 Eliceiri, K. W. & Huttenlocher, A. Distinct inflammatory and wound healing
1416 responses to complex caudal fin injuries of larval zebrafish. *Elife* **8**, (2019).
1417 102. Hoodless, L. J., Lucas, C. D., Duffin, R., Denvir, M. A., Haslett, C., Tucker, C.
1418 S. & Rossi, A. G. Genetic and pharmacological inhibition of CDK9 drives
1419 neutrophil apoptosis to resolve inflammation in zebrafish in vivo. *Sci. Rep.* **6**,
1420 36980 (2016).
1421 103. Burns, C. G. & MacRae, C. A. Purification of hearts from zebrafish embryos.
1422 *BioTechniques* vol. 40 274–282 (2006).
1423
1424 **Figures:**

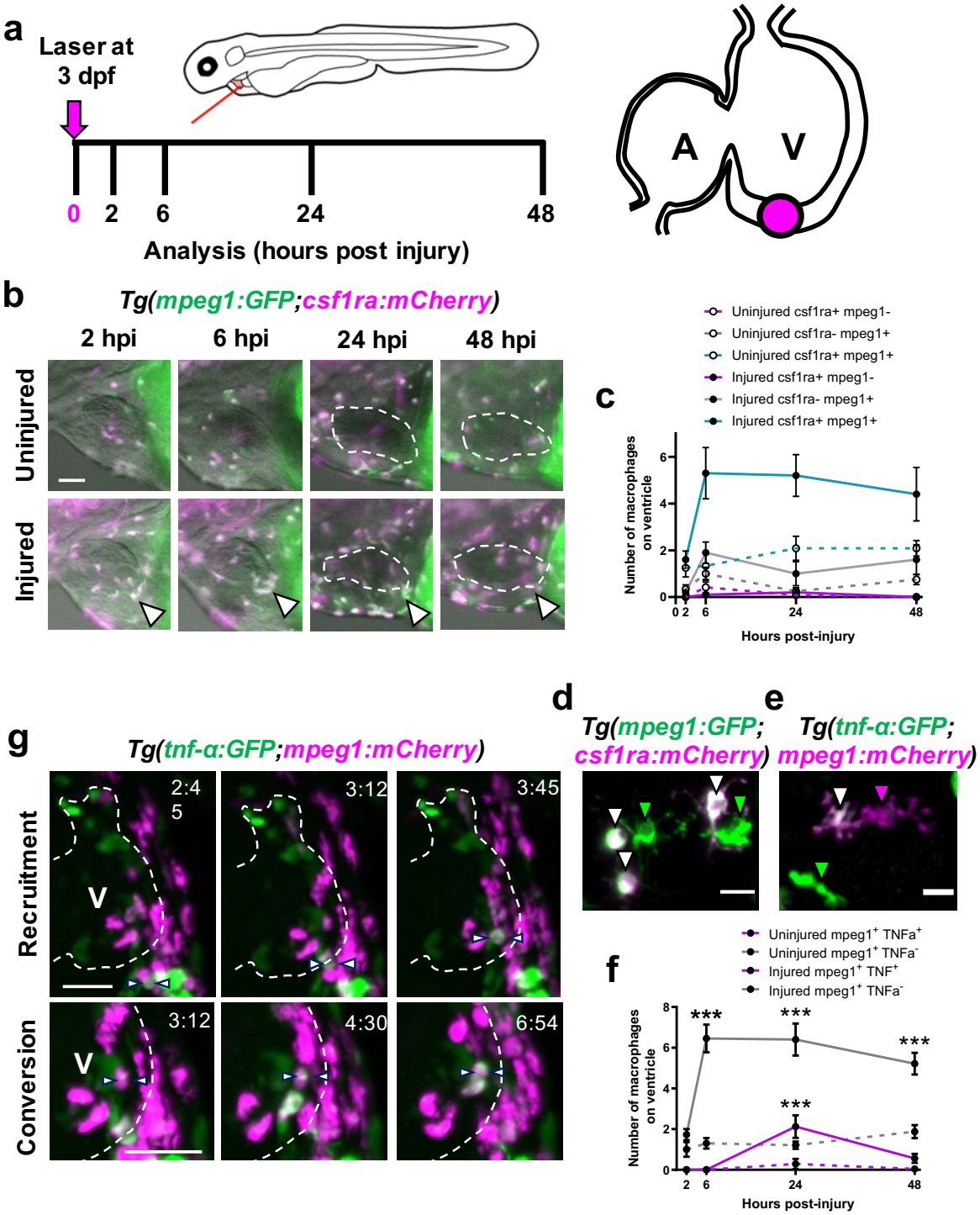

Figure 1: Cardiac macrophages display heterogeneity and plasticity following injury.

(a) Schematic illustrating the cardiac laser injury model with imaging timepoints marked (left) and the injury site at ventricular apex of a 3 dpf larval heart marked (magenta circle) (right). (b) Representative lateral view epifluorescence images of uninjured and injured hearts at the standard timepoints in *Tg(mpeg1:GFP;csf1ra:gal4;UAS:NfsB-mCherry)* (abbreviated to csf1ra:mCherry in

1433 all panels), white arrow = ventricular apex, dashed line = heart outline. (c)
1434 Quantification of number of csf1ra+mpeg1-, csf1ra-mpeg1+ and csf1ra+mpeg1+
1435 macrophages on the ventricle in uninjured and injured larvae at standard timepoints
1436 (n=10-12). (d) Representative epifluorescence image of csf1ra-mpeg1+ and
1437 csf1ra+mpeg1+ macrophages of different morphologies. (e) Representative
1438 epifluorescence image of tnf-*α*+mpeg1+ and tnf-*α*-mpeg1+ macrophages. (f)
1439 Quantification of number of tnf-*α*+mpeg1+ and tnf-*α*-mpeg1+ macrophages on the
1440 ventricle in uninjured and injured larvae at standard timepoints (n=10-25). (g) Time-
1441 lapse stills of injured *Tg(tnf-α:GFP;mpeg1:mCherry)* ventricles imaged live in the
1442 larvae by heart-synchronised light-sheet microscopy. Timestamps indicated, dashed
1443 line = ventricle outline, arrows = macrophage recruited as tnf-*α*+ (top) and
1444 macrophage converting to tnf-*α*+ (bottom). Scale bar = 50μm (b & g), 10μm (d & e).
1445 ***$p \leq 0.001$, 2way ANOVA followed by Holm-Sidak's Post-hoc test.
1446

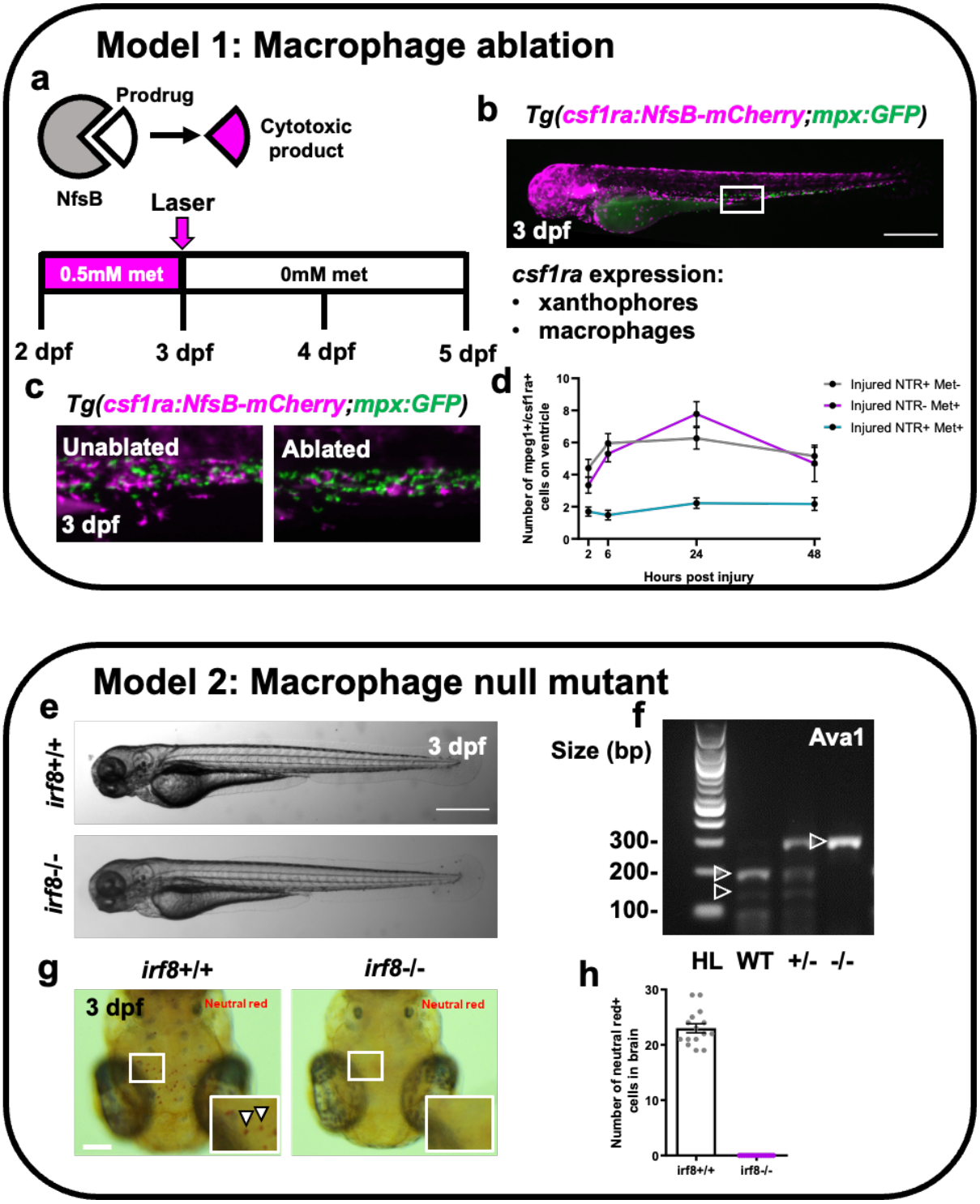

Figure 2: Macrophages can be pharmacologically ablated or developmentally blocked genetically.

(a) Schematic illustrating how nitroreductase enzyme 'NfsB' catabolises prodrug 'metronidazole' to form a cytotoxic biproduct. (b) Representative epifluorescence image of a *Tg(csf1ra:gal4;UAS:NfsB-mCherry;mpx:GFP*) 3 dpf larva (abbreviated to *Tg(csf1ra:mCherry;mpx:GFP)* in all panels), white box = caudal haematopoietic

1455 tissue, magenta = macrophages and green = neutrophils (CHT) (c) Representative
1456 images of ablated and unablated macrophages in the CHT, size and location
1457 indicated in (b)) in *Tg(csf1ra:mCherry;mpx:GFP)* 3dpf larvae. (d) Quantification of
1458 macrophages at standard timepoints, marked by either mpeg1 or csfr1a on the
1459 injured ventricle in eavh of the NTR=metronidazole ablation model's treatment
1460 groups NTR+Met-, NTR-Met+ and NTR+Met+.(e) Representative brightfield images
1461 of *irf8+/+* and *irf8-/-* larvae at 3 dpf. (f) Representative 1% agarose gel displaying
1462 Ava1 restriction digest band pattern for WT, irf8 heterozygous and homozygous
1463 mutants. (g) Representative dorsal view brightfield image of 3 dpf larval heads
1464 stained with neutral red vital dye with white zoom panel highlighting stained
1465 macrophages (microglia) (red) in *irf8+/+* but not *irf8-/-* larvae. (h) Quantification of the
1466 number of neutral red positive stained cells (macrophages/microglia) in larval brains
1467 of *irf8+/+* and *irf8-/-* at 3 dpf. Scale bar = 500μm (b & e), 100μm (g).
1468

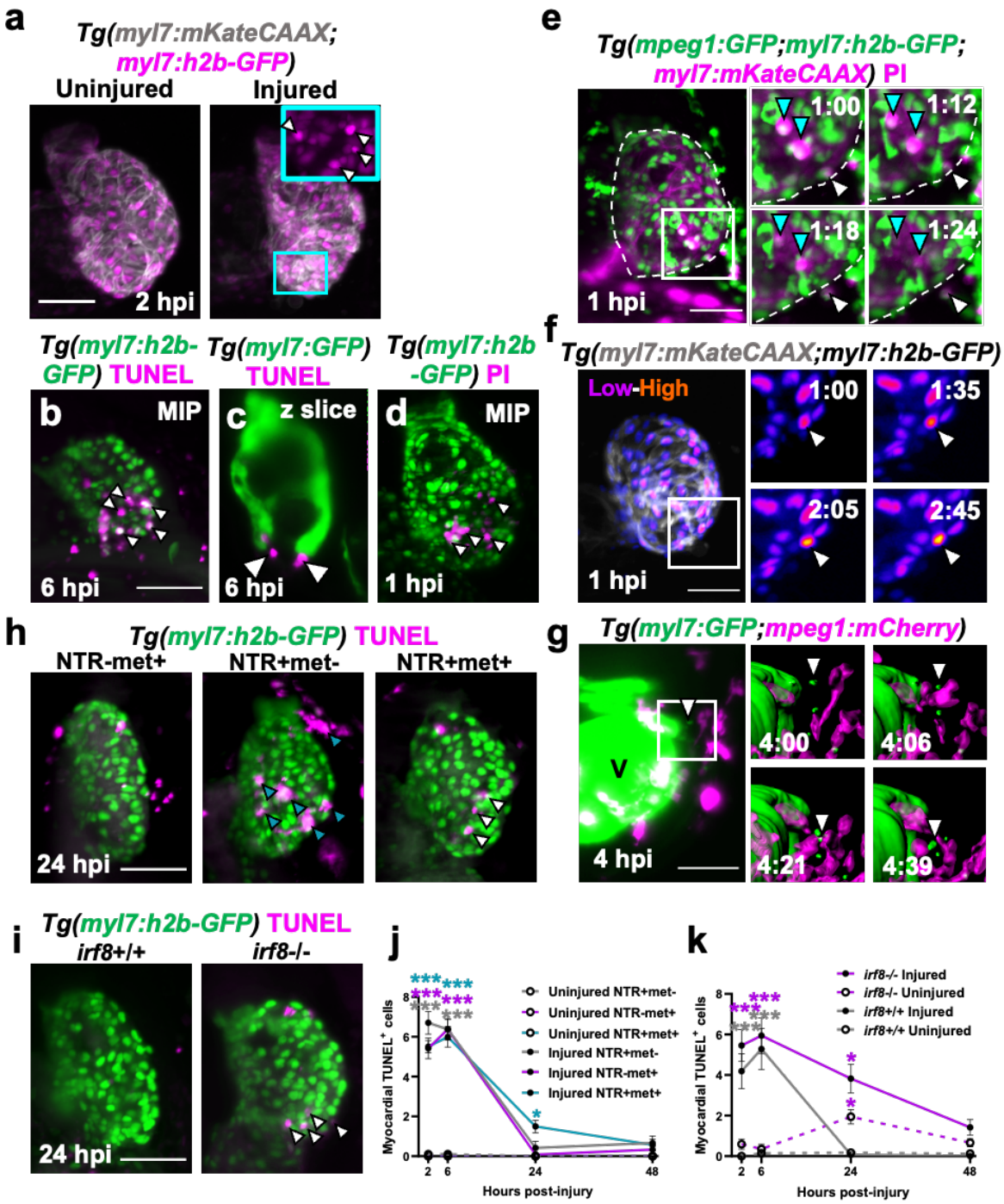

Figure 3: Macrophages are required for timely removal of apoptotic cardiomyocytes.

(a) Representative light-sheet-acquired images of uninjured and injured *Tg(myl7:h2b-GFP;myl7:mKateCAAX)* ventricles highlighting condensed nuclei in cyan outline zoom panel (white arrow-heads). (b) Representative light-sheet-acquired images of TUNEL stained hearts 6 hpi at in (b)*Tg(myl7:h2b-GFP)* and (c) *Tg(myl7:GFP)* larvae. White arrow-heads = apoptotic cardiomyocytes/myocardium.

1477 (d) Representative light-sheet-acquired image of a propidium iodide (PI) stained
1478 *Tg(myl7:h2b-GFP)* heart 1 hpi. White arrow-heads = necrotic debris. (e) Time-lapse
1479 stills of injured *Tg(myl7:h2b-GFP;myl7:mKateCAAX;mpeg1:GFP)* ventricles imaged
1480 from 1 hpi by heart-synchronised light-sheet imaging. Round GFP^{low} =
1481 cardiomyocyte nuclei and stellate GFP^{high} =macrophages. Cyan arrow-heads =
1482 Necrotic cardiomyocyte nuclei and white arrow-heads = expelled necrotic
1483 cardiomyocyte, white box = zoom panel. (f) Time-lapse stills of injured *Tg(myl7:h2b-*
1484 *GFP;myl7:mKateCAAX)* ventricles imaged from 1 hpi. GFP intensity show by heat
1485 LUT, white arrow-head = apoptotic cardiomyocyte/condensing nucleus, white box =
1486 zoom panel. (g) Time-lapse stills of an injured *Tg(myl7:GFP;mpeg1:mCherry)*
1487 ventricle from 4 hpi where the full size panel has high gain in the GFP channel to
1488 highlight GFP^{low} myocardial debris and zoom panels (area indicated by white box)
1489 are surface rendered to highlight removal of myocardium (green) by macrophages
1490 (magenta). V = high gain ventricle, white arrow-head = myocardial debris. (h)
1491 Representative light-sheet acquired images of injured *Tg(myl7:h2b-*
1492 *GFP;csfr1a:gal4;UAS:NfsB-mCherry)* ventricles per macrophage ablation model
1493 injury group at 24 hpi. Cyan arrow-heads = Macrophages and white arrow-heads =
1494 TUNEL+ cells. (i) Representative light-sheet acquired images of *irf8+/+* and *irf8-/-*
1495 *Tg(myl7:h2b-GFP)* hearts stained by TUNEL at 24 hpi. White arrow-heads =
1496 TUNEL+ cells. (j) Quantification of TUNEL+ myocardial cells in uninjured and injured
1497 *Tg(myl7:h2b-GFP;csfr1a:gal4;UAS:NfsB-mCherry)* ventricles per macrophage
1498 ablation group. n=1-12 (k) Quantification of TUNEL+ myocardial cells in uninjured
1499 and injured, *irf8+/+* and *irf8-/- Tg(myl7:h2b-GFP)* ventricles. n=15-29. Scale bars =
1500 50 μm, $*p \leq 0.05$, $**p \leq 0.01$, $***p \leq 0.001$ 2way ANOVA followed by Holm-Sidak's Post-
1501 hoc tests.
1502

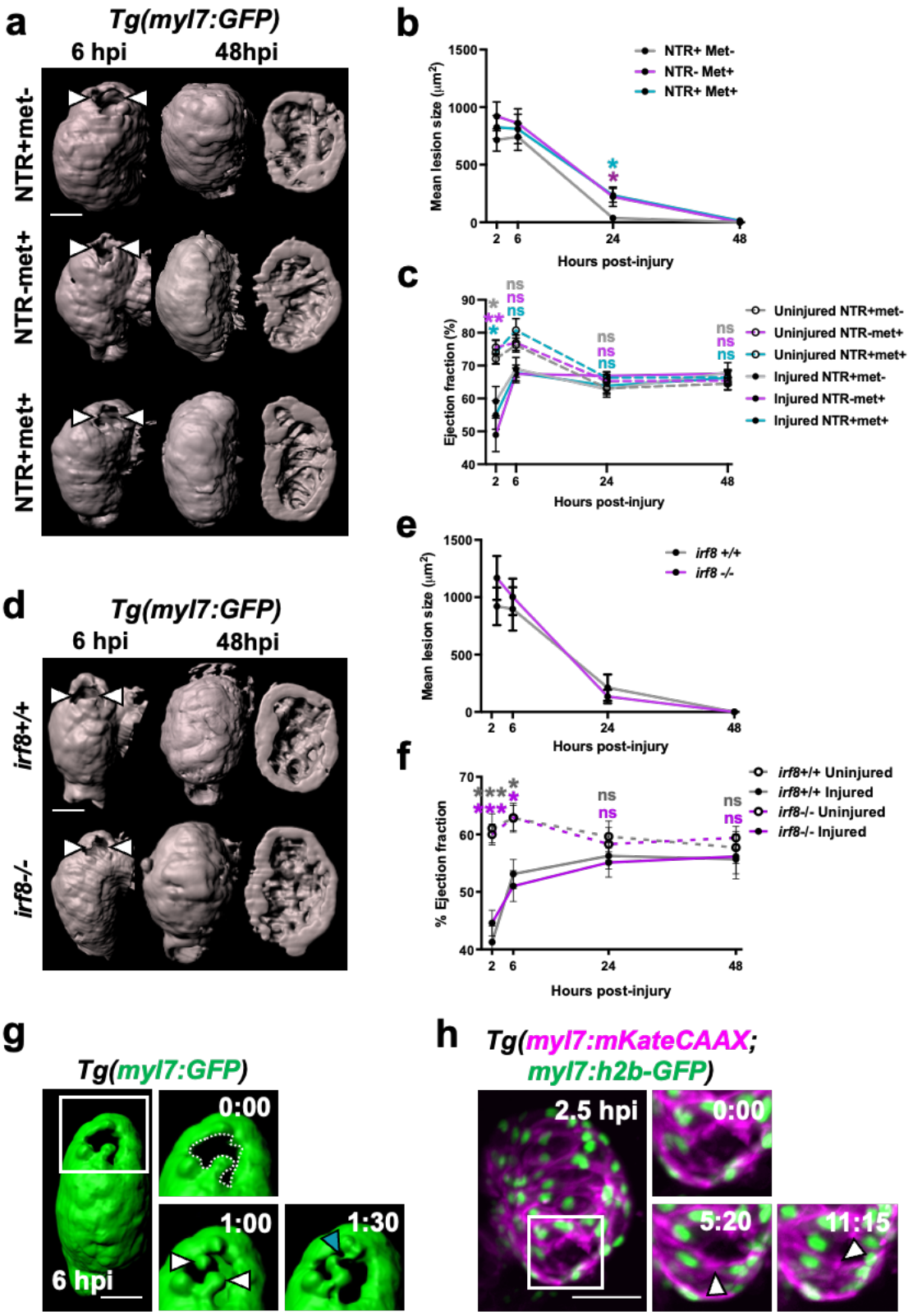

Figure 4: Macrophages not required for the recovery of cardiac structure or function.

1507 (a) Representative GFP surface-renders of light-sheet-acquired z-stacks of injured
1508 ventricles from *Tg(myl7:GFP;csfr1a:gal4;UAS:NfsB-mCherry)* larvae, macrophage
1509 ablation groups as indicated in the figure. Abluminal myocardial surface is shown at
1510 6 hpi (left) and abluminal and luminal surfaces shown at 48 hpi following
1511 regeneration (middle & right). White arrow-heads = laser lesion. (b) Quantification of
1512 mean lesion size in injured *Tg(myl7:GFP;csfr1a:gal4;UAS:NfsB-mCherry)* larvae per
1513 macrophage ablation group. n=11-22. (c) Quantification of ventricular ejection
1514 fraction % in uninjured and injured *Tg(myl7:GFP;csfr1a:gal4;UAS:NfsB-mCherry)*
1515 larvae per macrophage ablation group, n=10-12. (d) Representative GFP surface-
1516 renders of light-sheet-acquired z-stacks of injured ventricles from *irf8+/+* and *irf8-/-*
1517 *Tg(myl7:GFP)* larvae. Abluminal myocardial surface is shown at 6 hpi (left) and
1518 abluminal and luminal surfaces shown at 48 hpi following regeneration (middle &
1519 right). White arrow-heads = laser lesion. (e) Quantification of mean lesion size in
1520 injured *irf8+/+* and *irf8-/- Tg(myl7:GFP)* larvae, n=15. (f) Quantification of ventricular
1521 ejection fraction % in uninjured and injured *irf8+/+* and *irf8-/- Tg(myl7:GFP)* larvae
1522 n=15-20. (g) Time-lapse GFP-surface-rendered stills of an injured *Tg(myl7:GFP)*
1523 ventricle from 6 hpi. White box = zoom panel, white arrow-heads = myocardial buds,
1524 cyan arrow-head = myocardial bridge. (h) Time-lapse stills of an injured
1525 *Tg(myl7:mKateCAAX;myl7:h2b-GFP)* ventricle from 2.5 hpi. White box = zoom
1526 panel, white arrow-heads = cell-cell junctions *$p \leq 0.05$, ***$p \leq 0.001$ 2way ANOVA
1527 followed by Holm-Sidak's Post-hoc tests. Scale bars = 50 μm
1528

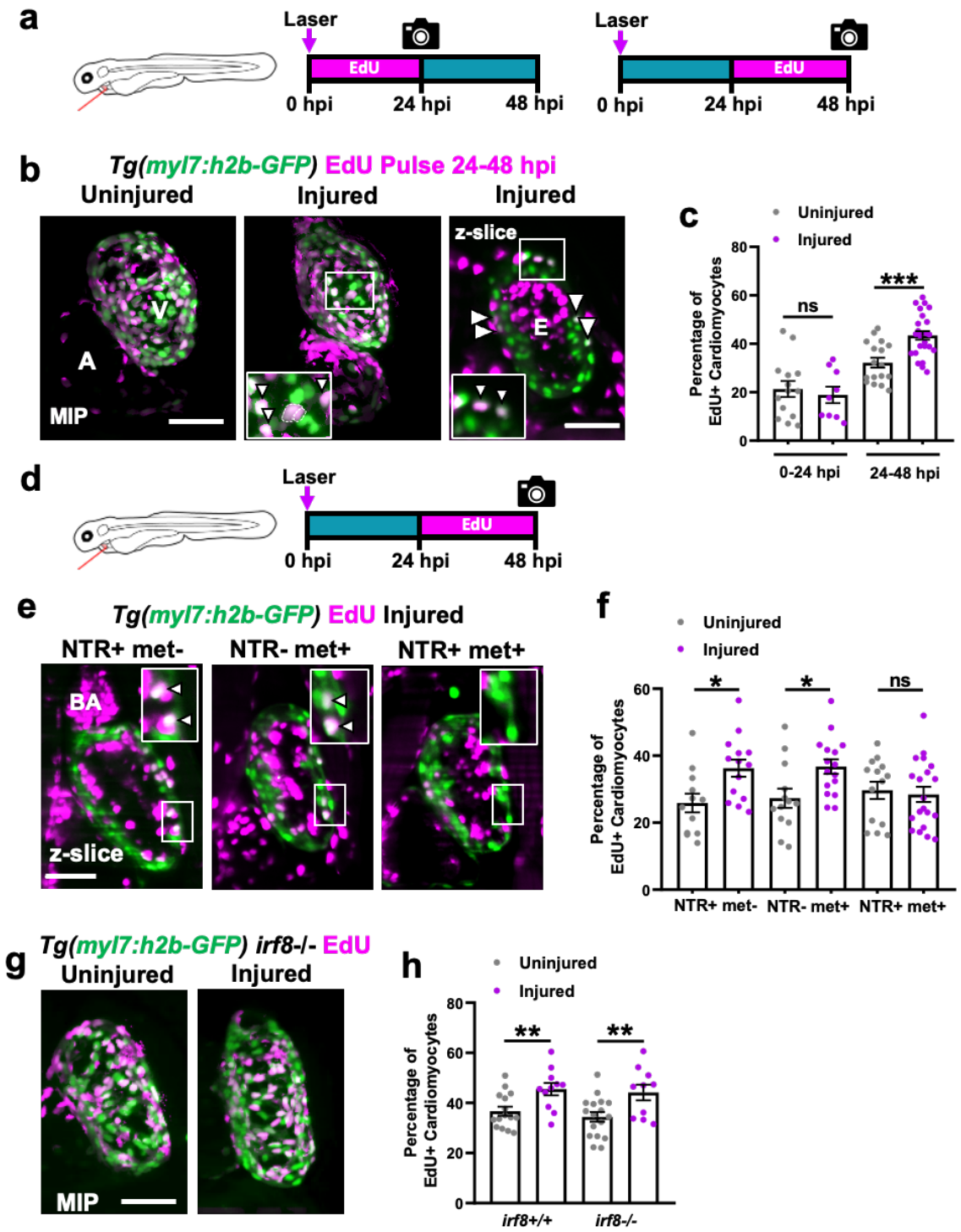

Figure 5: Macrophage ablation abolishes injury-dependent cardiomyocyte proliferation.

(a) Schematic illustrating EdU pulse strategy for labelling proliferating cardiomyocytes over 0-24 hpi (left) and 24-48 hpi (right). (b) Representative images of EdU-stained hearts from *Tg(myl7:h2b-GFP)* acquired by light-sheet microscopy at 48 hpi. Non-myocardial EdU signal is excluded post-acquistionally to allow

1536 interpretable maximal intensity projections (MIPs). A = atrium, v = ventricle, white
1537 boxes = zoom panels, white arrow-heads = EdU+ cardiomyocyte nuclei and dashed
1538 line = outline of dividing cardiomyocyte daughter nuclei. (c) Quantification of the
1539 percentage of ventricular EdU+ cardiomyocytes in uninjured and injured
1540 *Tg(myl7:h2b-GFP)* hearts pulsed over 0-24 hpi or 24-48 hpi. ****p≤0.001* Unpaired t
1541 test. (d) Schematic illustrating EdU pulse strategy for labelling proliferating
1542 cardiomyocytes over 24-48 hpi in *Tg(myl7:h2b-GFP;csfr1a:gal4;UAS:NfsB-mCherry)*
1543 larvae per standard macrophage ablation groups. (e) Representative images of EdU-
1544 stained hearts from *Tg(myl7:h2b-GFP;csfr1a:gal4;UAS:NfsB-mCherry)* acquired by
1545 light-sheet microscopy at 48 hpi. White boxes = zoom panels, white arrow-heads =
1546 EdU+ cardiomyocyte nuclei and BA = bulbous arteriosus. (f) Quantification of the
1547 percentage of ventricular EdU+ cardiomyocytes in uninjured and injured
1548 *Tg(myl7:h2b-GFP;csfr1a:gal4;UAS:NfsB-mCherry)* hearts pulsed over 24-48 hpi.
1549 **p≤0.05* Kruskal-Wallis test and Dunn's multiple comparison Post-hoc test. (g)
1550 Representative images of uninjured and injured EdU-stained hearts from *irf8-/-*
1551 *Tg(myl7:h2b-GFP)* acquired by light-sheet microscopy at 48 hpi. Non-myocardial
1552 EdU signal is excluded post-acquistionally to allow interpretable maximal intensity
1553 projections (MIPs). (h) Quantification of the percentage of ventricular EdU+
1554 cardiomyocytes in uninjured and injured *irf8+/+* and *irf8-/- Tg(myl7:h2b-GFP)* hearts
1555 pulsed 24-48 hpi. Scale bars = 50 μm. ***p≤0.01* Unpaired t test
1556

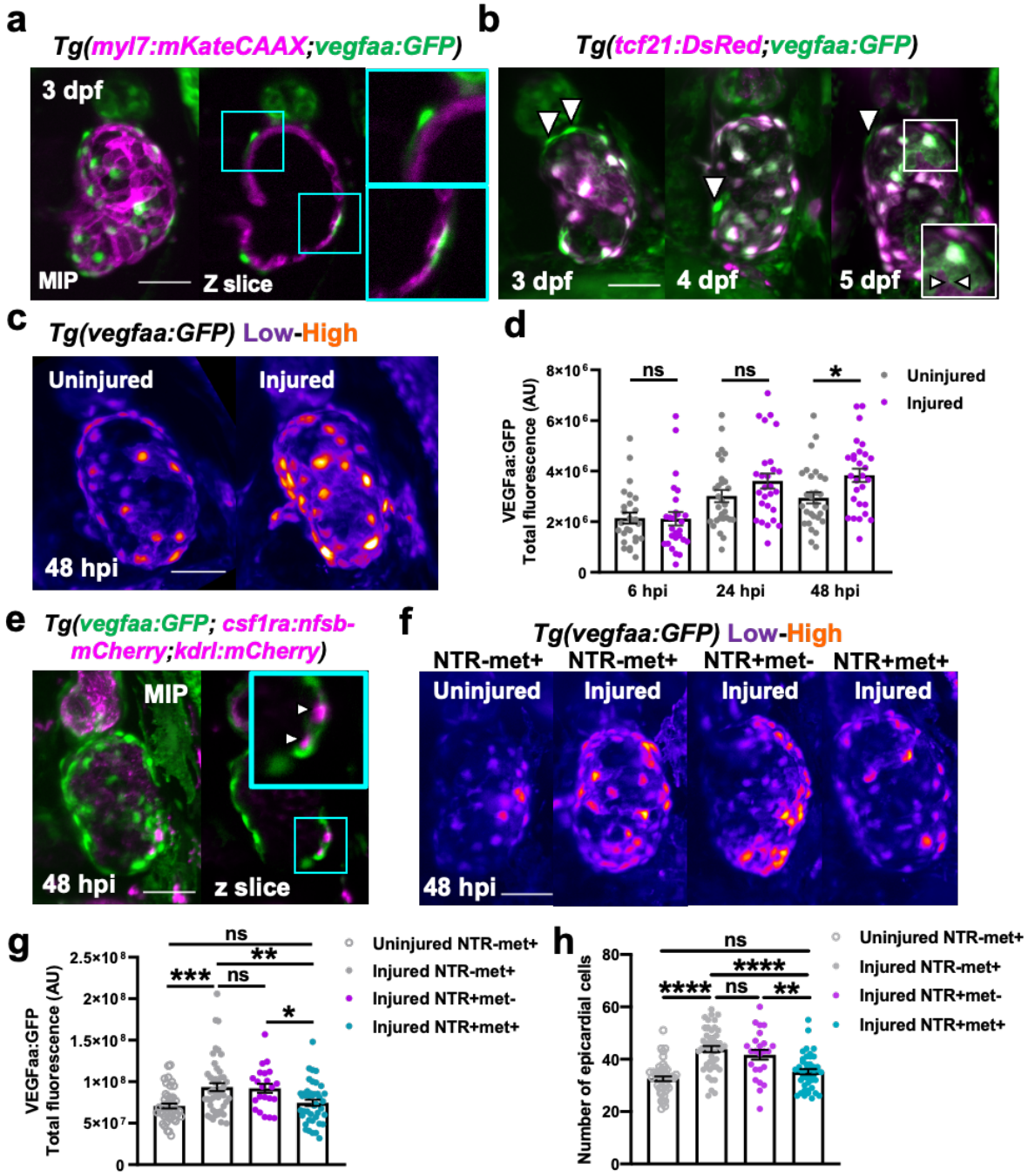

Figure 6: Macrophages stimulate epicardial expansion following cardiac injury. (a) Representative image of an uninjured 3 dpf ventricle from a *Tg(myl7:mKateCAAX;myl7:h2b-GFP)* larva acquired by light-sheet microscopy showing vegfaa+ cells (green) overlying myocardium (magenta). Cyan box = zoom panel. (b) Representative images of 3, 4 and 5 dpf ventricles from a *Tg(tcf21:DsRed;vegfaa:GFP)* larvae acquired by light-sheet microscopy showing high colocalization of vegfaa with epicardial marker tcf21. White arrow-heads =

1566 vegfaa+tcf21- epicardial cells and white box = zoom panel. (c) Representative
1567 images of uninjured and injured ventricles from *Tg(vegfaa:GFP)* larvae acquired at
1568 48 hpi by light-sheet microscopy. Heat LUT applied to highlight increased intensity of
1569 epicardial vegfaa:GFP in injured hearts. (d) Quantification of total ventricular
1570 VEGFaa:GFP fluorescence in uninjured and injured hearts over standard injury
1571 model timepoints, n=28-30. *$p \leq 0.05$ One way ANOVA followed by Holms-Sidak's
1572 multiple comparison Post-hoc tests. (e) Representative image of a ventricle from a
1573 *Tg(vegfaa:GFP;csfr1a:gal4;UAS:NfsB-mCherry;kdrl:hsa.HRAS-mCherry)* 48 hpi
1574 showing macrophages in the epicardial-myocardial niche (white arrow-heads). Cyan
1575 box = zoom panel. (f) Representative images of uninjured and injured ventricles from
1576 *Tg(vegfaa:GFP;csfr1a:gal4;UAS:NfsB-mCherry)* larvae from metronidazole-
1577 nitroreductase macrophage ablation groups at 48 hpi. A heat LUT is applied to
1578 highlight increase in overall fluorescence in injured groups besides NTR+met+. (g)
1579 Quantification of total vegfaa:GFP fluorescence (g) and epicardial cell number (h) in
1580 uninjured and injured ventricles from *Tg(vegfaa:GFP;csfr1a:gal4;UAS:NfsB-*
1581 *mCherry)* larvae from metronidazole-nitroreductase macrophage ablation groups at
1582 48 hpi. Scale bars = 50 μm, n=46. *$p \leq 0.05$, **$p \leq 0.01$, ***$p \leq 0.001$ One way ANOVA
1583 followed by Holms-Sidak's multiple comparison Post-hoc tests.
1584

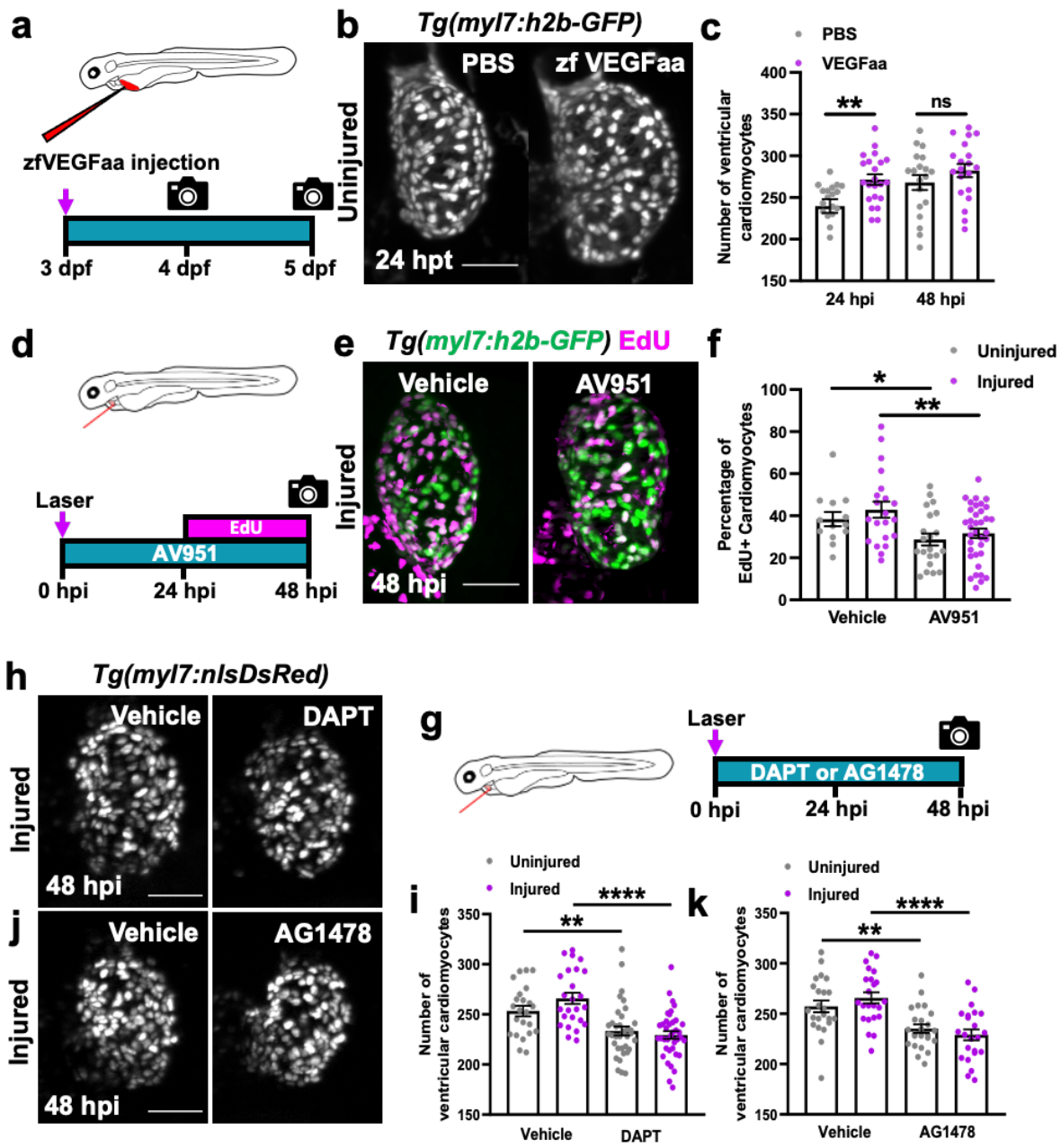

Figure 7: VEGFaa signalling is both sufficient and necessary to drive cardiomyocyte proliferation.

(a) Schematic illustrating zfVEGFaa treatment strategy via microinjection into the common cardinal vein of uninjured larvae at 72 hpi. (b) Representative light-sheet-acquired images of *Tg(myl7:h2b-GFP)* larvae at 24 hpi treated with PBS 0.1% BSA or zfVEGFaa 0.1% BSA injection. (c) Quantification of ventricular cardiomyocyte number in *Tg(myl7:h2b-GFP)* larvae at 24 and 48 hpi treated with PBS 0.1% BSA or zfVEGFaa 0.1% BSA injection, n=20. ***p≤0.01* unpaired t test. (d) Schematic illustrating AV951 treatment and EdU pulsing strategy for uninjured and injured larvae. (e) Representative images of injured ventricles from *Tg(myl7:h2b-GFP)*

1596 larvae, EdU stained and bathed in vehicle or AV951, imaged at 48 hpi by light-sheet
1597 microscopy. Non-myocardial EdU signal is excluded post-acquistionally to allow
1598 interpretable maximal intensity projections (MIPs). (f) Quantification of the
1599 percentage of EdU+ cardiomyocyte nuclei from uninjured and injured ventricles from
1600 *Tg(myl7:h2b-GFP)* larvae, EdU stained and bathed in vehicle or AV951, n=13-36.
1601 *$p \leq 0.05$, **$p \leq 0.01$ unpaired t test. (g) Schematic illustrating the treatment strategy for
1602 DAPT and AV951 bathing of uninjured and injured larvae. (h) Representative images
1603 of injured *Tg(myl7:nlsDsRed)* larvae treated with vehicle or DAPT, acquired at 48 hpi
1604 by light-sheet microscopy. (i) Quantification of ventricular cardiomyocyte number in
1605 uninjured and injured *Tg(myl7:h2b-GFP)* larvae at 48 hpi treated with vehicle or
1606 DAPT, n=24-40. **$p \leq 0.01$, ****$p \leq 0.0001$ Unpaired t test.(j) Representative images of
1607 injured *Tg(myl7:nlsDsRed)* larvae treated with vehicle or AG1478, acquired at 48 hpi
1608 by light-sheet microscopy. (k) Quantification of ventricular cardiomyocyte number in
1609 uninjured and injured *Tg(myl7:h2b-GFP)* larvae at 48 hpi treated with vehicle or
1610 AG1478, n=24. **$p \leq 0.01$, ****$p \leq 0.0001$ Unpaired t test. Scale bars = 50 μm.
1611

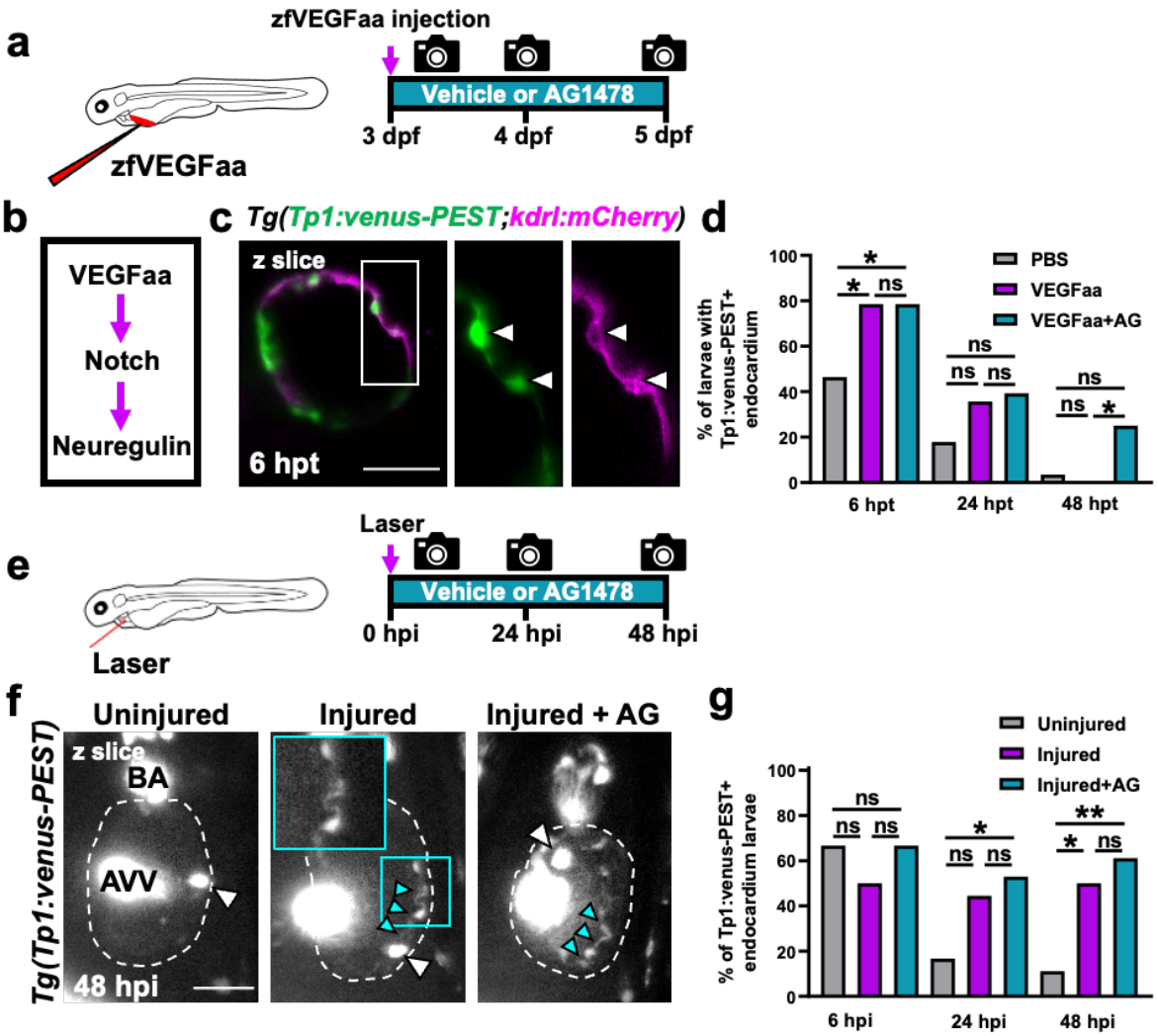

Figure 8: VEGFaa acts upstream of endocardial notch signalling. (a) Schematic illustrating the treatment strategy for the injection of uninjured larvae with zfVEGFaa and continuous bathing in AG1478 solution. (b) Hypothesised signalling pathway active in uninjured and injured larval hearts driving cardiomyocyte proliferation. (c) Representative light-sheet-acquired z plane showing notch expression colocalising with endocardium in *Tg(Tp1:venus-PEST;kdrl:hsa.HRAS-mCherry),* abbreviated in the figure to *Tg(Tp1:venus-PEST;kdrl:has.HRAS-mCherry).* AG1478 abbreviated to AG, white box = zoom panel. (d) Quantification of the proportion of larvae with notch+ endocardium at 6, 24, and 48 hpt following zfVEGFaa injection and bathing in AG1478, n=28. *$p \leq 0.05$ Fisher's exact test. (e) Schematic illustrating the treatment strategy for the lasering of larvae and continuous bathing in AG1478 solution. (f) Representative z plane images of uninjured, injured and injured AG-treated ventricles from *Tg(tp1:venus-PEST)* larvae acquired by light-sheet microscopy at 48 hpi. BA = bulbous arteriosus, AVV = atrioventricular valve,

1627 white arrow-heads =laterally inhibited cardiomyocytes, cyan arrow-heads = notch+
1628 endocardium and cyan box = zoom panel. (g) Quantification of the proportion of
1629 larvae with notch+ endocardium at 6, 24, and 48 hpt following laser injury and
1630 bathing in AG1478, n=18. *$p \leq 0.05$, **$p \leq 0.01$ Fisher's exact test. Scale bars = 50 μm.
1631

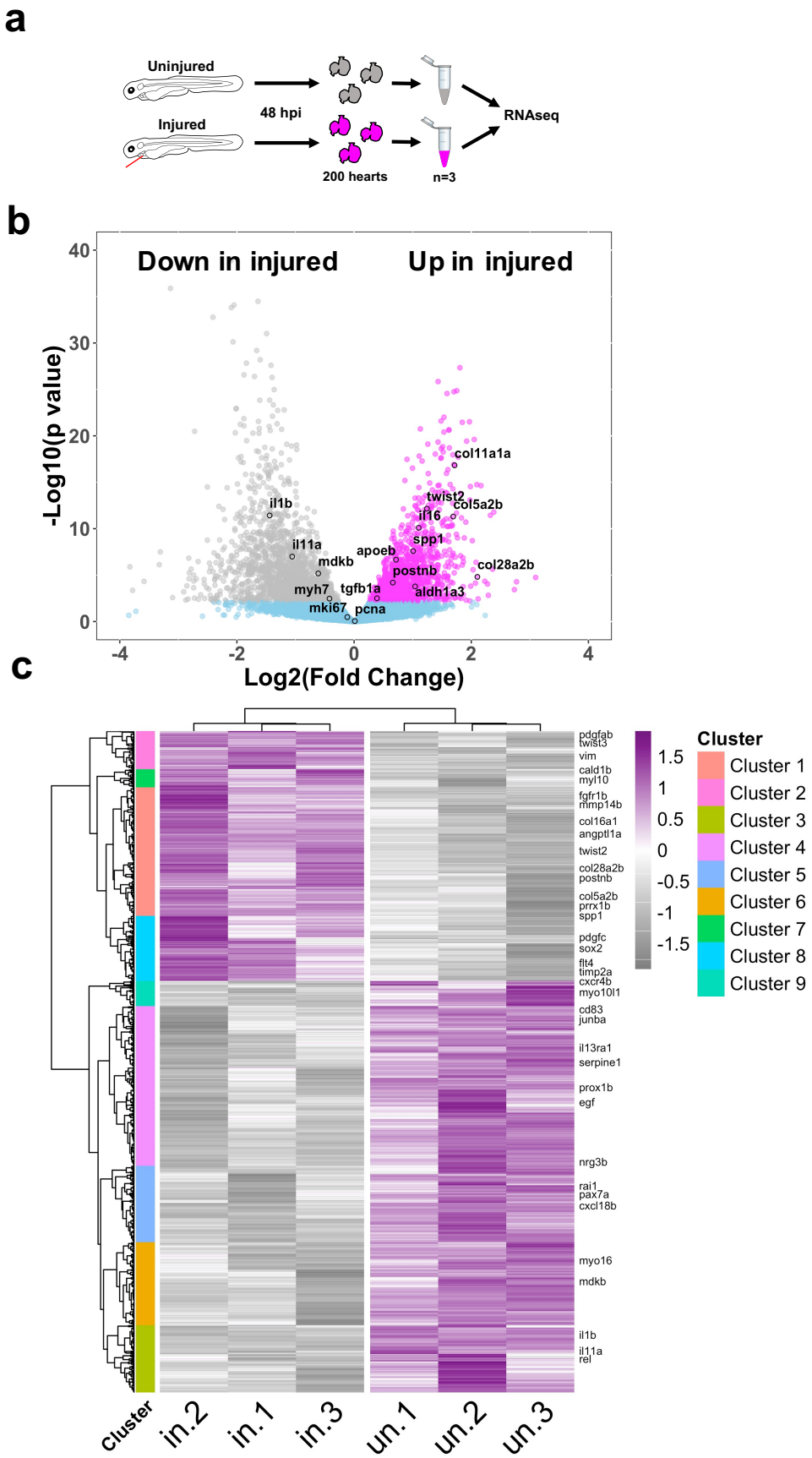

Figure 9: RNAseq analysis of larval hearts following injury

(a) Schematic illustrating the extraction of uninjured and injured hearts at 48 hpi and the pooling of 200 hearts per biological replicate for RNAseq. n=3 (b) Volcano plot showing the Log_2(Fold Change) and $-Log_{10}$(p value) for transcripts of each detected gene. Genes whose adjusted p values fall below 0.05 are deemed statistically non-significant and coloured blue. Genes up regulated in injured hearts are coloured magenta and those upregulated in uninjured hearts are coloured grey. (c) Heatmap displaying statistically significantly differentially expressed genes with a Log_2(Fold Change) >0.5. Genes were hierarchically clustered by Pearson correlation with z scaling. Clusters are indicated on the left with their dendrogram. Magenta = high expression and grey = low expression. Genes with relevance to cardiac regeneration are highlighted as annotations on the right of the plot. n=3

Supplementary figures:

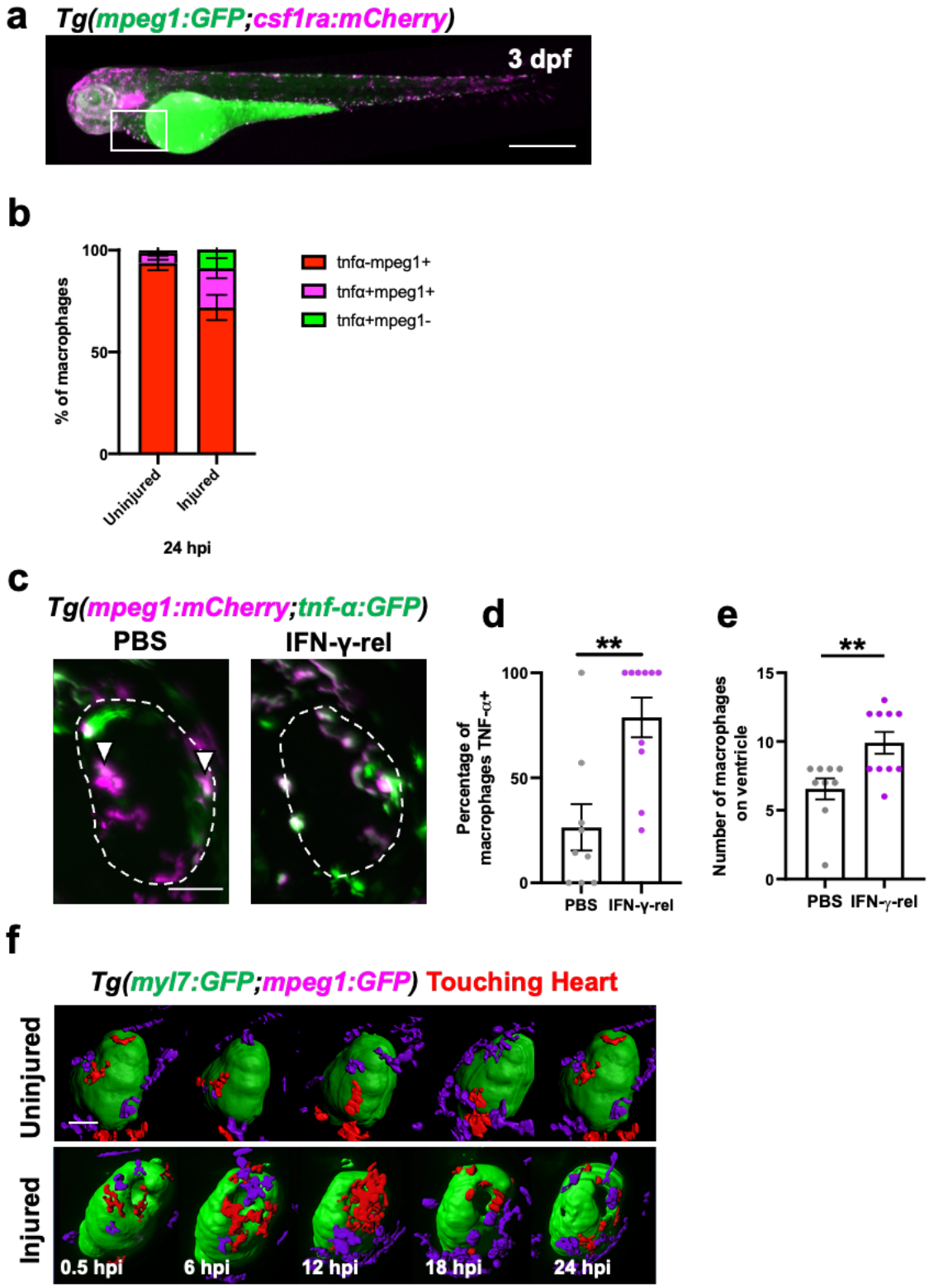

Supplementary figure 1: Cardiac macrophage phenotype in larval zebrafish is plastic and can be polarised to TNF-α+ by IFN-γ-rel.

(a) Representative epifluorescence image of a 3 dpf *Tg(mpeg1:GFP;csf1ra:gal4;UAS:NfsB-mCherry)* abbreviated to

Tg(mpeg1:GFP;csf1ra:mCherry) in the figure showing an anterior-posterior polarity in macrophage expression of csf1ra (csf1ra marking higher proportion of anterior macrophages). White box = indicated pericardial area. Scale bar = 500μm. (b) Quantification of the proportion of macrophages that are tnfα-mpeg1+, tnfα+mpeg1+ and tnfα+mpeg1- on hearts in uninured and injured larvae at 24 hpi. (c) Representative images of hearts from *Tg(mpeg1:mCherry;tnf-α:GFP)* larvae at 24 hpi injected with PBS or IFN-γ-rel. White dashed line = outline of the ventricle and white arrow-heads = tnfa+mpeg1+ macrophages. Scale bar = 50μm. (d) Quantification of the proportion of tnf-*α*+ macrophages on hearts at 24 hpi upon injection at 0 hpi with PBS or IFN-γ-rel. (e) Quantification of the number of macrophages on the injured ventricle at 24 hpi upon injection at 0 hpi with PBS or IFN-γ-rel. (f) Time-lapse stills of *Tg(myl7:GFP;mpeg1:mCherry)* hearts acquired by heart-synchronised light-sheet microscopy, surface rendered and colour coded to show myocardium in green, macrophages on the heart in red and macrophages elsewhere in purple. Macrophages can be seen to change from stellaet to rounded over time following injury. Scale bar = 50μm.

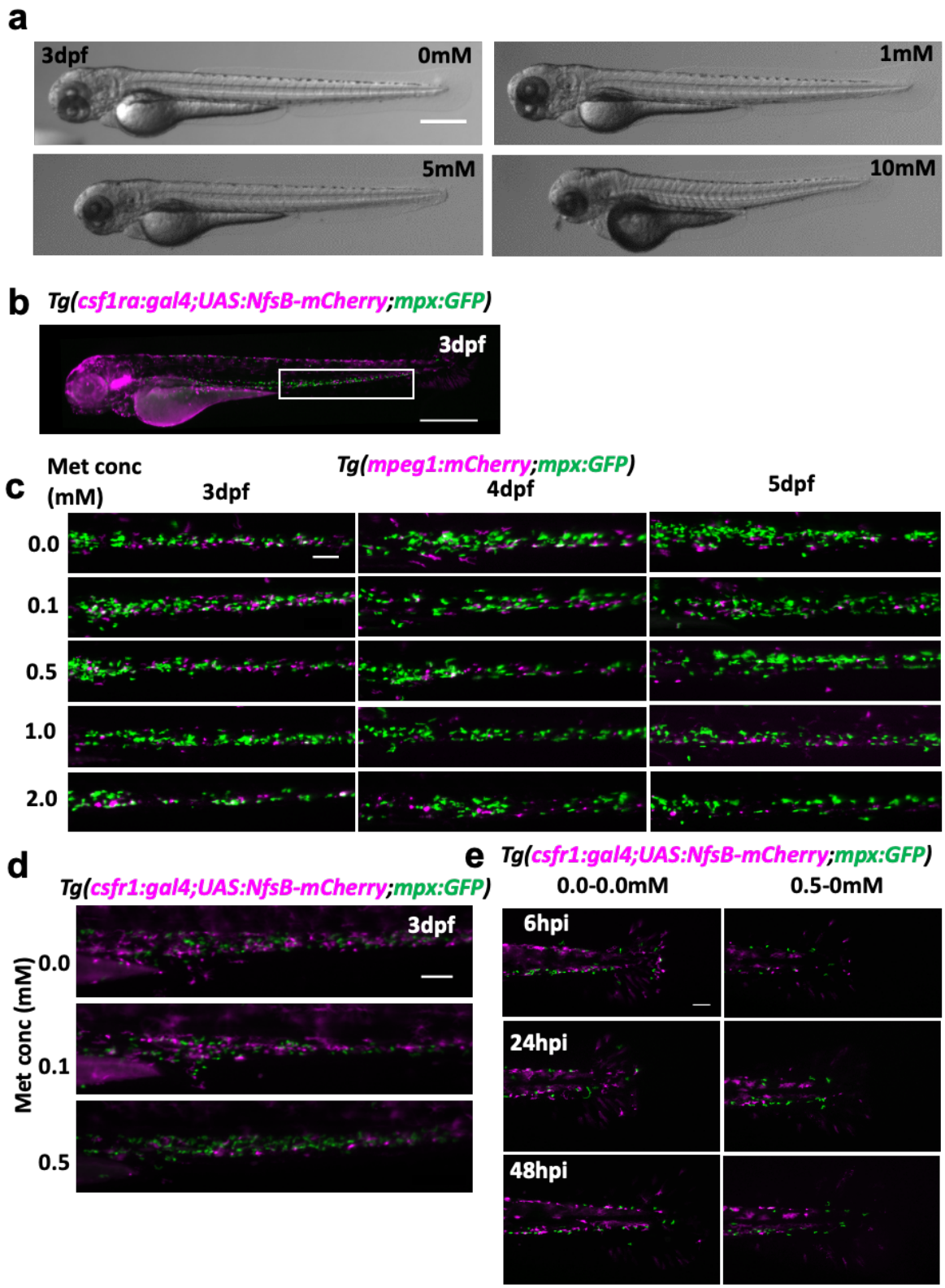

Supplementary figure 2: Optimisation of metronidazole dose for macrophage ablation.

(a) Representative brightfield images of larvae phenotype after incubation in the concentrations of metronidazole 2-3 dpf indicated in the figure. Scale bar = 500μm.

1680 (b) Representative epifluorescence image of a 3 dpf *Tg(csf1ra:gal4;UAS:NfsB-*
1681 *mCherry;mpx:GFP)* larva, white box = zoom panel, scale bar = 500μm. (c)
1682 Representative epifluorescence images of CHT (region indicated by white box in (b))
1683 at 3, 4 and 5 dpf following treatment with metronidazole (concentrations indicated in
1684 figure) 2-3 dpf. Neutrophils = green and macrophages = magenta. No NTR
1685 expression therefore toxicity to immune cells can be assessed, scale bar = 100μm
1686 (d) Representative epifluorescence images of the CHT in *Tg(csf1ra:gal4;UAS:NfsB-*
1687 *mCherry;mpx:GFP)* larvae incubated in the doses of metronidazole indicated in the
1688 figure 2-3 dpf. Scale bar = 100μm. (e) Representative epifluorescence images of
1689 *Tg(csf1ra:gal4;UAS:NfsB-mCherry;mpx:GFP)* tail fins resected at 72 hpi following
1690 incubation in 0.5mM metronidazole or vehicle (0mM). The macrophage response
1691 (magenta) can be seen to be blocked only in the metronidazole treated group
1692 whereas the neutrophil response is unaffected. Scale bar = 100μm.
1693

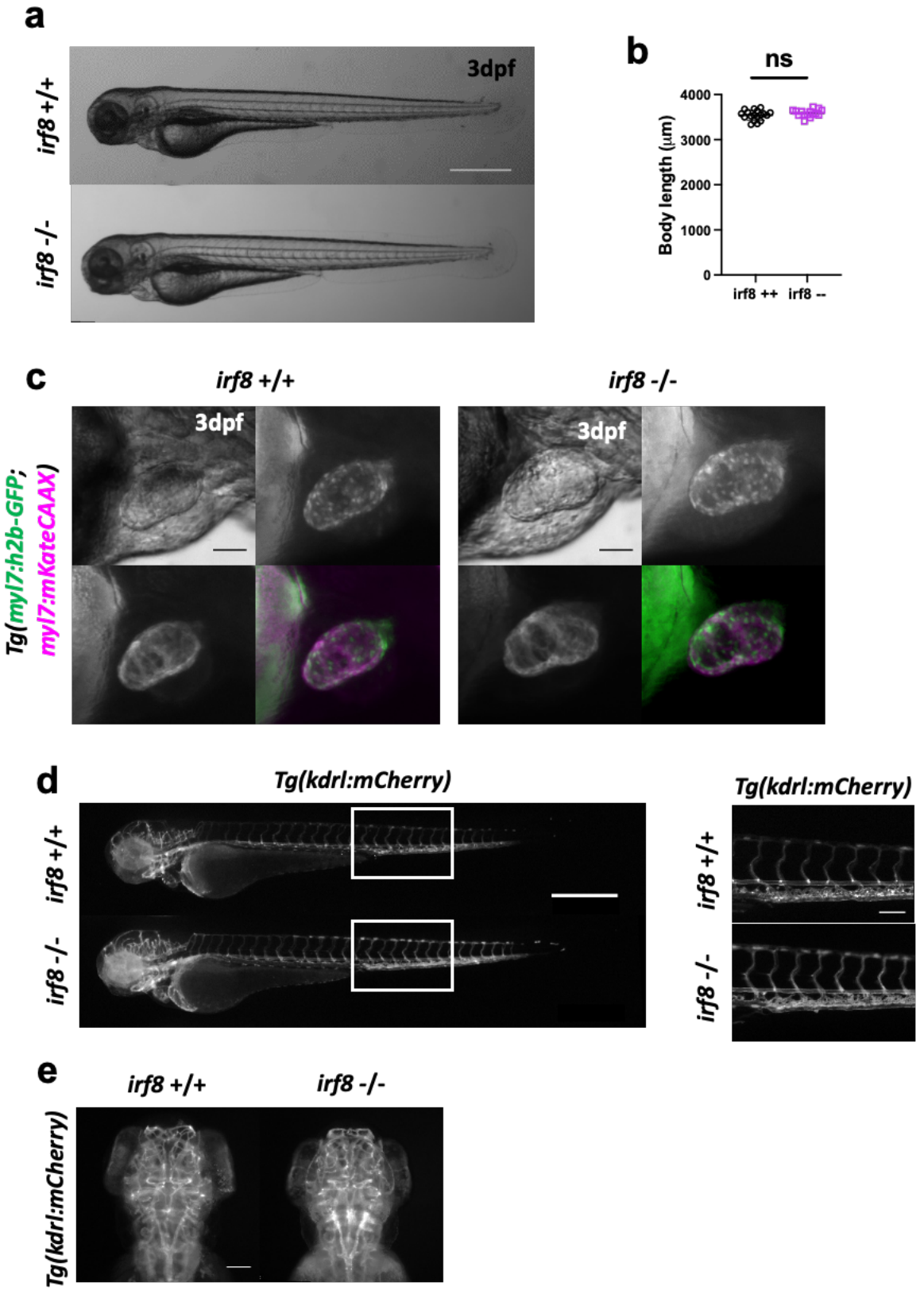

Supplementary figure 3: *irf8-/-* mutants show no overt adverse phenotype. (a) Brightfield whole larvae image showing no morphological difference between *irf8-/-* and *irf8+/+* at 3 dpf, scale bar = 500μm. (b) Quantification of body length in *irf8+/+*

1698 and *irf8-/-* showing no difference between genotypes. (c) Brightfield and
1699 epifluorescence images of a laterally viewed heart from *irf8+/+ and irf8-/-*
1700 *Tg(myl7:h2b-GFP;myl7:mKateCAAX)* larvae at 3 dpf showing no cardiac
1701 abnormalities in *irf8-/-* larvae. Scale bar = 50μm (d) Epifluorescence whole larvae
1702 image of *irf8+/+ and irf8-/- Tg(kdrl:mCherry)* larvae showing no vascular
1703 abnormalities in *irf8-/-* larvae. Scale bar = 500μm. White boxes = zoom panels (right,
1704 scale bar = 100μm). (e) Dorsal view representative epifluorescence images of cranial
1705 vasculature in *Tg(kdrl:mCherry)* showing no difference between *irf8+/+* and *irf8-/-*
1706 larvae, scale bar = 100μm.
1707

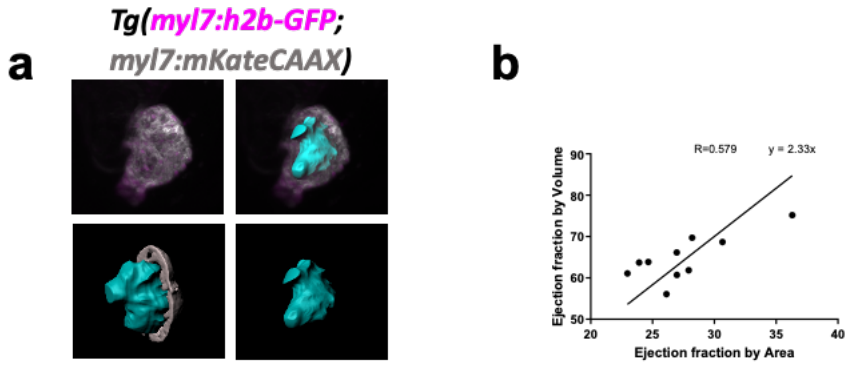

1708
1709 **Supplementary figure 4: Ejection fraction by area is proportional to ejection**
1710 **fraction by volume.**
1711 (a) Representative IMARIS-generated image showing a rendered ventricular
1712 myocardium (grey render), rendered chamber volume (cyan) and MIP of 3D heart
1713 synchronised light-sheet scan of a 3 dpf heart (ventricle) in diastole. Image acquired
1714 from a *Tg(myl7:h2b-GFP;myl7:mKateCAAX)* larva. (b) Quantification of ejection
1715 fraction by area (calculated by diastolic and systolic lateral brightfield) and by volume
1716 (calculated by surface renders of luminal volumes in diastole and systole) per fish.
1717

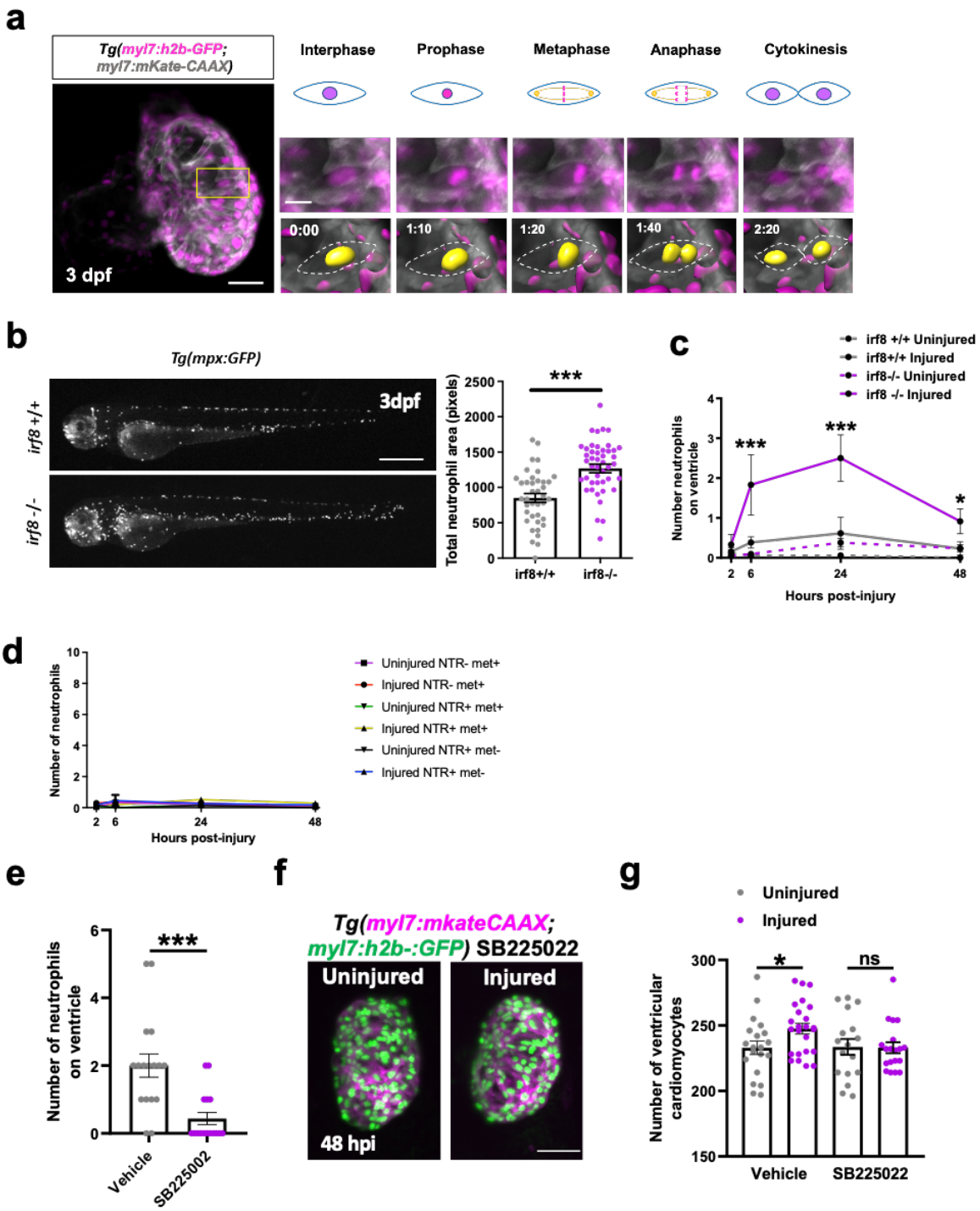

Supplementary figure 5: *irf8-/-* larvae have a larger neutrophil response to cardiac injury than *irf8+/+*.

(a) Representative stills from heart synchronised light-sheet timelapse of a laser injured 3 dpf *Tg(myl7:h2b-GFP;myl7:mKateCAAX)* larva showing an example of each phase of complete cell division of a single cardiomyocyte, typical of larval hearts. Yellow box = zoom panel, left scale bar = 30 μm and right scale bar = 10 μm. Timestamps post-injury indicated in figure. (b) Representative whole larva

epifluorescence image of *irf8-/-* and *irf8+/+ Tg(mpx:GFP)* larvae showing *irf8-/-* to have greater global neutrophil numbers (scale bar = 500 μm), quantified in the graph (right). ****p≤0.001.* t test, n=39-46. (c) Quantification of neutrophil numbers at the ventricle in uninjured and injured *irf8+/+* and *irf8-/-* larvae at the standard laser-injury model timepoints showing *irf8-/-* larvae to have a significantly greater neutrophil response, n=17-25. (d) Quantification of neutrophil numbers at the ventricle in uninjured and injured NTR-met+, NTR+met+ and NTR+met- larvae at the standard laser-injury model timepoints showing all metronidazole-nitroreductase treatment groups to have a minimal neutrophil response and therefore no neutrophil compensation in the macrophage ablated group NTR+met+, n=17-24. (e) Quantification of the number of recruited neutrophils at the injured ventricle in at 24 hpi in *Tg(myl7:h2b-GFP;myl7:mKateCAAX)* larvae bathed in vehicle or SB225002 -2 to 24 hpi showing SB225002 to significantly reduce neutrophil number, n=17. (f) Representative light-sheet acquired images of uninjured and injured *irf8-/- Tg(myl7:h2b-GFP;myl7:mKateCAAX)* ventricles at 48 hpi following treatment with SB225002 -2 to 24 hpi, scale bar = 50 μm. (g) Quantification of ventricular cardiomyocyte number in uninjured and injured *irf8-/- Tg(yl7:h2b-GFP;myl7:mKateCAAX)* ventricles at 48 hpi following treatment with vehicle or SB225002 -2 to 24 hpi, n=17-20, **p≤0.05.* t test

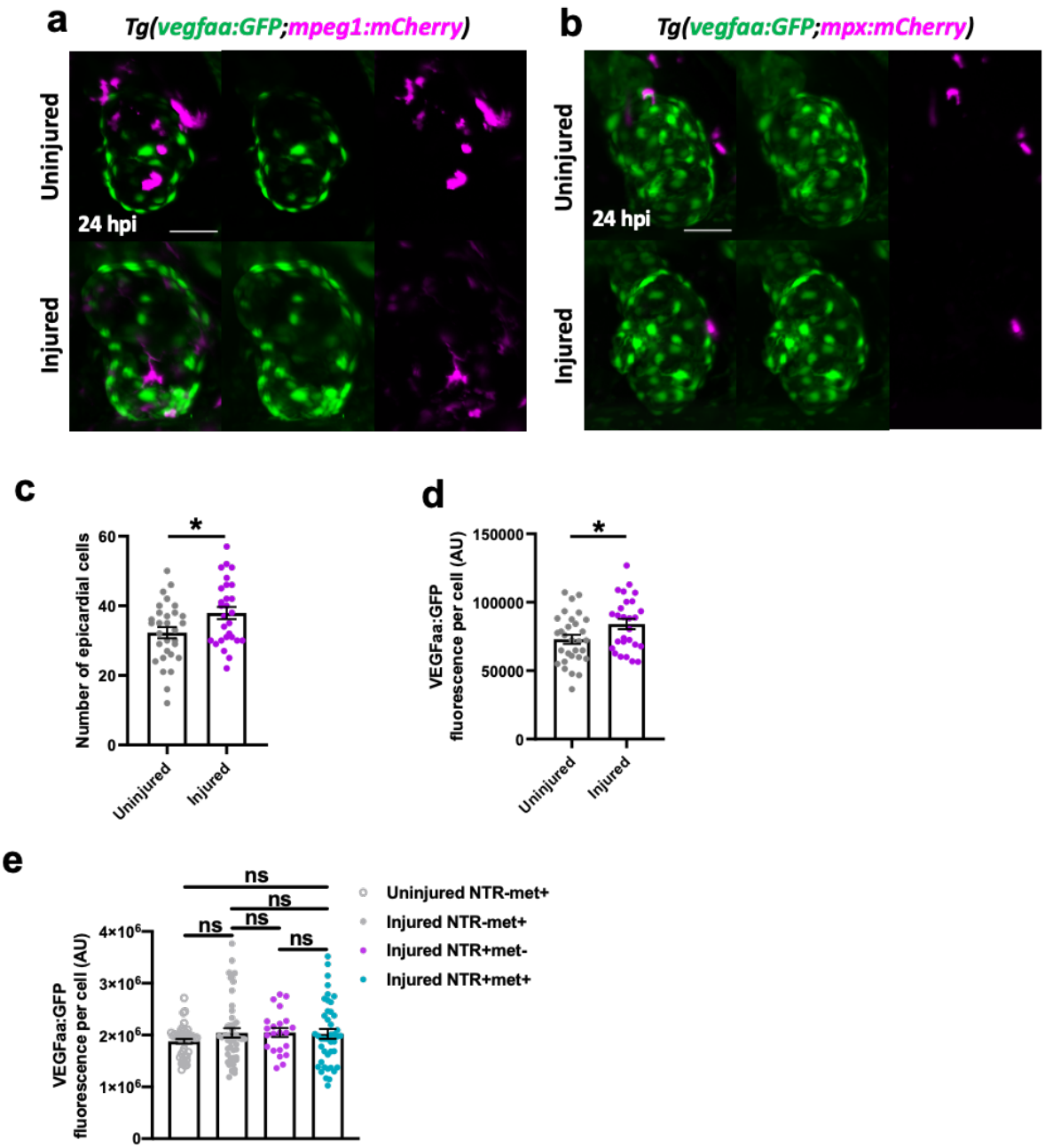

Supplementary figure 6: vegfaa:GFP expression does not colocalize with macrophages or neutrophils following larval heart injury.

(a) Representative light-sheet-acquired image of an injured *Tg(vegfaa:GFP;mpeg1:mCherry)* heart 24 hpi showing VEGFaa expression only in the epicardium and not in macrophages, scale bar = 100μm. (b) Representative light-sheet-acquired image of an injured *Tg(vegfaa:GFP;mpx:mCherry)* heart 24 hpi showing VEGFaa expression only in the epicardium and not in neutrophils, scale bar = 100μm. (c) Quantification of the number of epicardial cells, as marked by

1756 vegfaa:GFP, on injured ventricles at 48 hpi in uninjured and injured larvae, n=30.
1757 *$p \leq 0.05$ t test (d) Quantification of the average vegfaa:GFP expression of epicardial
1758 cells per cell, on injured ventricles at 48 hpi in uninjured and injured larvae, n=30.
1759 *$p \leq 0.05$ t test (e) Quantification of average vegfaa:GFP fluorescence per cell in
1760 metronidazole-nitroreductase ablation model groups at 48 hpi, n=22-44. One-way
1761 ANOVA followed by Holm-Sidak's multiple comparisons Post-hoc test.
1762

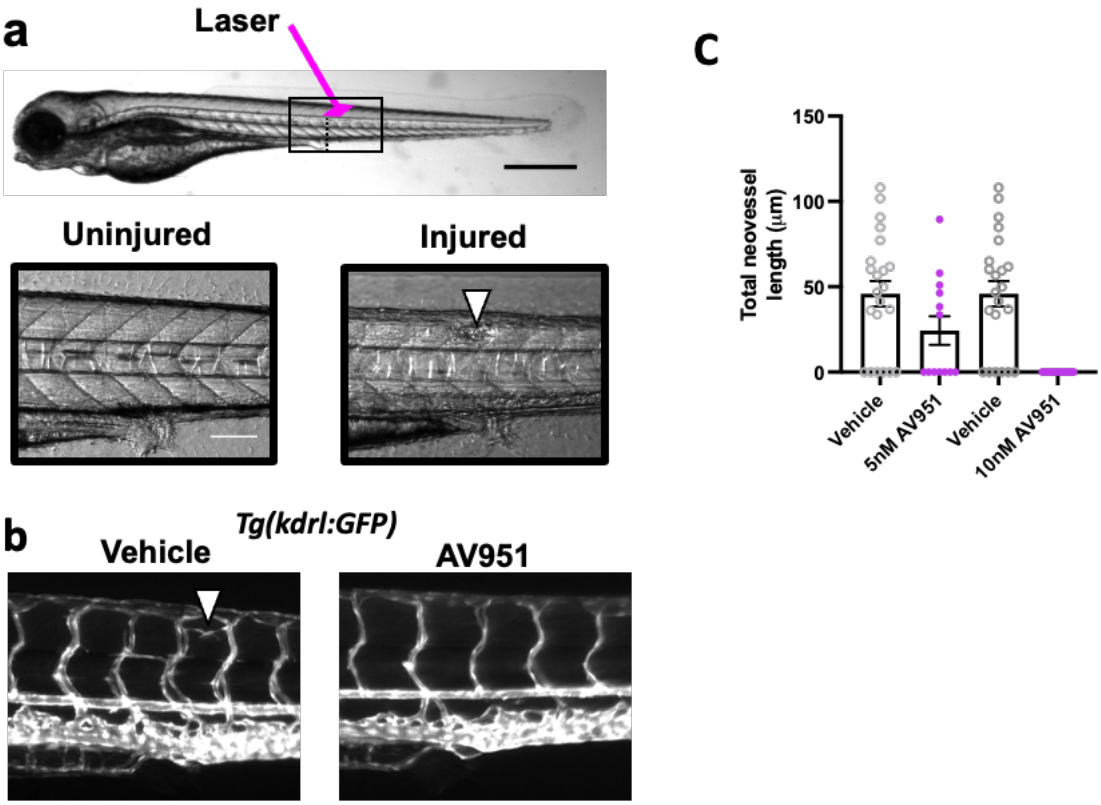

1763
1764
1765
1766 **Supplementary figure 7: 10nM VEGFR pan antagonist AV951 entirely abolishes**
1767 **inflammatory angiogenesis.**
1768 (a) Annotated brightfield image of a 3 dpf whole larva (0 hpi) with the somite used for
1769 laser injury highlighted in magenta, scale bar = 500μm .Black box = zoom panel for
1770 lower panels. Lower panels show the laser lesion site (white arrow), scale bar =
1771 100μm. (b) Representative epifluorescence images of trunk vasculature surrounding
1772 the laser lesioned muscle segment/somite in vehicle and 10nM AV951 treated (0-48
1773 hpi) larvae at 48 hpi. White arrow = neovasculature. (c) Quantification of

neovasculature length at 48 hpi after laser injury for vehicle, 5 nM and 10nM AV951-treated larvae, n=13-22.

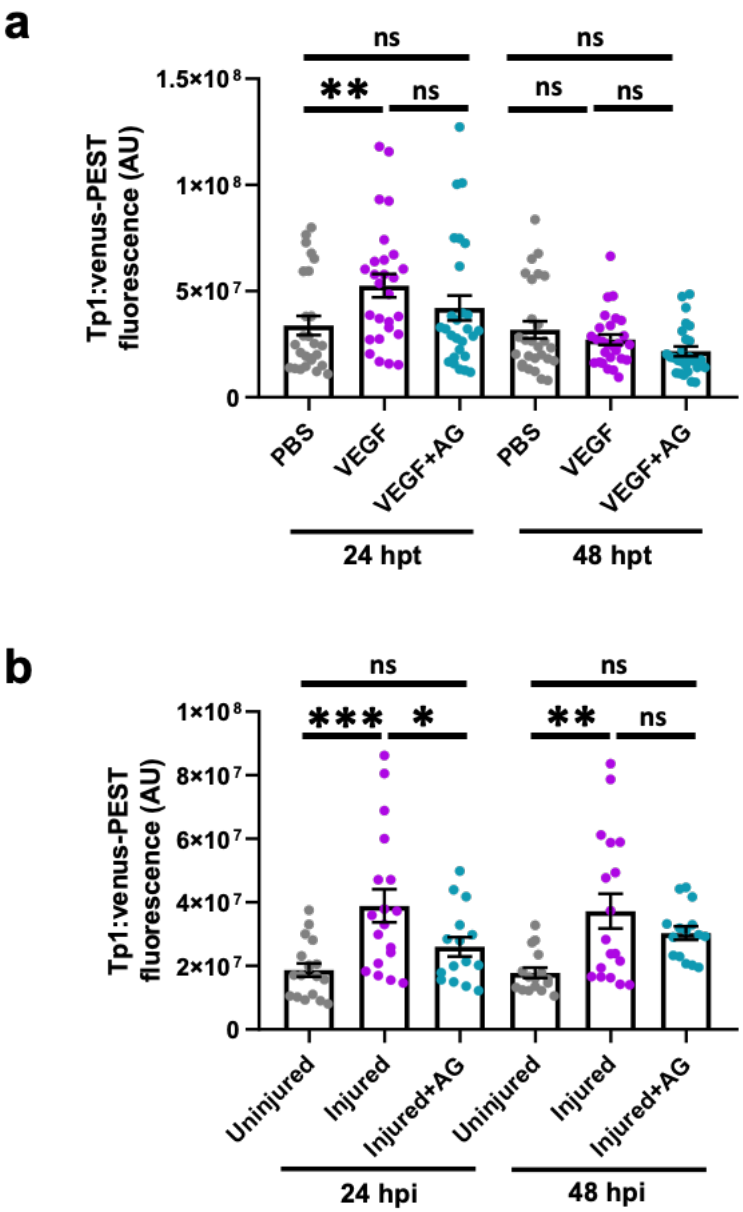

Supplementary figure 8: VEGFaa injection and injury increase myocardial notch signaling in a Nrg-ERRB dependent manner.

(a) Quantification of total ventricular myocardial from *Tg(Tp1:venus-PEST)* hearts following injection with PBS or zfVEGFaa or injection with zfVEGFaa and incubation in pan ERRB antagonist AG1478, n=28 (b) Quantification of total ventricular myocardial from *Tg(Tp1:venus-PEST)* uninjured hearts and in hearts following laser injury or laser injury and in pan ERRB antagonist AG1478, n=18. *$p \leq 0.05$, **$p \leq 0.01$,

***p≤0.001,* One way ANOVA followed by Holm-Sidak's multiple comparisons Post-hoc test.

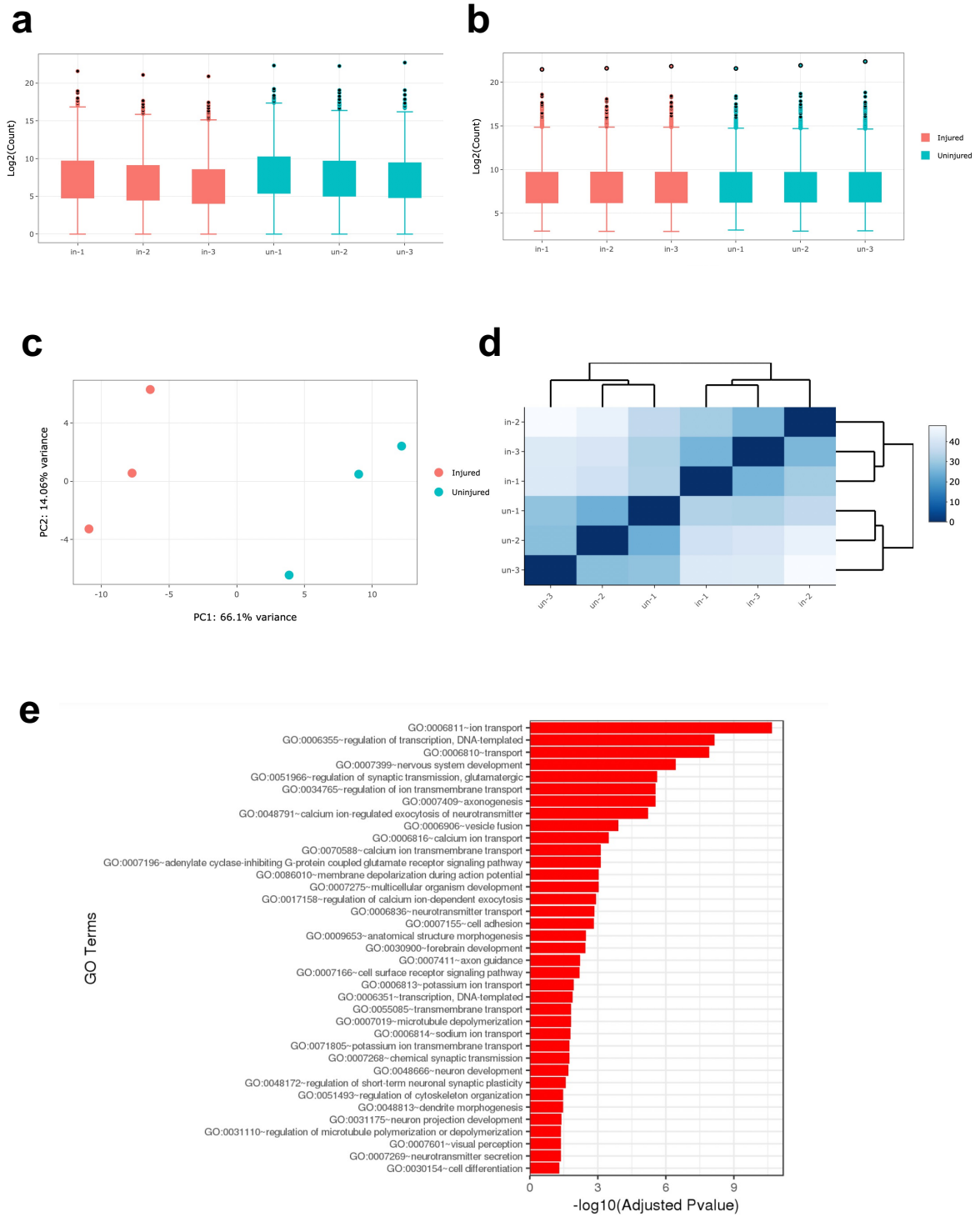

Supplementary figure 9: Bulk RNAseq analysis of uninjured and injured larval hearts

1791 (a) Box plot illustrating the distribution of reads before (a) and after normalisation (b).
1792 (c) Principle component analysis of samples illustrating sample similarity. (d)
1793 Distance matrix illustrating pairwise sample similarity. (e) Plot showing gene ontology
1794 terms that were significantly enriched by Fishers exact test for significantly
1795 (padj<0.05) differentially expressed genes between uninjured and injured hearts at
1796 48. hpi.
1797
1798 **Videos:**
1799
1800 Videos 1-8 can be found deposited on Dropbox via the following link:
1801 https://www.dropbox.com/s/h91m523wiab6kh0/Videos.zip?dl=0
1802
1803 Video 1: LSFM-acquired heartbeat-synchronised timelapse of a
1804 *Tg(csf1ra:mCherry;mpeg1:GFP)* heart showing macrophage heterogeneity following
1805 cardiac injury.
1806 Video 2: LSFM-acquired heartbeat-synchronised timelapse of a
1807 *Tg(mpeg1:mCherry;tnfa:GFP)* heart showing macrophage plasticity following cardiac
1808 injury.
1809 Video 3: LSFM-acquired heartbeat-synchronised timelapse of a *Tg(myl7:h2b-*
1810 *GFP;mpeg1:GFP)* heart injected with propdium iodide showing PI+ cardiomyocyte
1811 expulsion following cardiac injury.
1812 Video 4: LSFM-acquired heartbeat-synchronised timelapse of a *Tg(myl7:h2b-*
1813 *GFP;myl7:mKateCAAX)* heart following cardiac injury showing cardiomyocyte
1814 apoptosis following injury.
1815 Video 5: LSFM-acquired heartbeat-synchronised timelapse of a
1816 *Tg(myl7:GFP;mpeg1:mCherry)* heart, 3D surface rendered, showing removal and
1817 internalization of myocardial debris by macrophages following injury.
1818 Video 6: LSFM-acquired heartbeat-synchronised timelapse of a *Tg(myl7:GFP)* heart,
1819 3D surface rendered, showing budding and bridging of wound margin myocardium
1820 following injury.
1821 Video 7: LSFM-acquired heartbeat-synchronised timelapse of a *Tg(myl7:h2b-*
1822 *GFP;myl7:mKateCAAX)* heart, showing budding and bridging of individual wound-
1823 margin cardiomyocytes following injury.

1824 Video 8: LSFM-acquired heartbeat-synchronised timelapse of a *Tg(myl7:h2b-*
1825 *GFP;myl7:mKateCAAX)* heart, showing cardiomyocyte cell division with nuclear
1826 division and cytokinesis.
1827
1828
1829
1830